Engineering *Pseudomonas putida* KT2440 towards in vivo implementation of a synthetic CO_2 fixation pathway

A Thesis

submitted to

Indian Institute of Science Education and Research Pune in partial fulfilment of the requirements for the BS-MS Dual Degree Programme

by

Jogindh SS

Indian Institute of Science Education and Research Pune

Dr. Homi Bhabha Road,

Pashan, Pune 411008, INDIA.

Date: April, 2025

Under the guidance of

Supervisor: Tobias Erb,

Max Planck Institute for Terrestrial Microbiology

From June 2024 to Mar 2025

INDIAN INSTITUTE OF SCIENCE EDUCATION AND RESEARCH PUNE

Certificate

This is to certify that this dissertation entitled **"Engineering *Pseudomonas putida* KT2440 towards in vivo implementation of a synthetic CO2 fixation pathway"** towards the partial fulfilment of the BS-MS dual degree programme at the Indian Institute of Science Education and Research, Pune represents study/work carried out by Jogindh SS at the Max Planck Institute for Terrestrial Microbiology under the supervision of Tobias J Erb, Director, Department of Biochemistry and Synthetic Metabolism, during the academic year 2024-2025.

Tobias J Erb

This thesis is dedicated to my family and friends

Declaration

I hereby declare that the matter embodied in the report entitled “Engineering *Pseudomonas putida* KT2440 towards in vivo implementation of a synthetic CO2 fixation pathway” are the results of the work carried out by me at the Department of Biochemistry and Synthetic Metabolism, Max Planck Institute for Terrestrial Microbiology, under the supervision of Dr Tobias Erb, and the same has not been submitted elsewhere for any other degree. Wherever others contribute, every effort is made to indicate this clearly, with due reference to the literature and acknowledgement of collaborative research and discussions.

Jogindh SS

20201079

Table of Contents

List of Tables

List of Figures

Abstract

As atmospheric CO2 levels continue to rise, threatening global climate stability, carbon fixation cycles offer a promising dual solution: they not only help reduce greenhouse gas concentrations but also provide a sustainable pathway to produce valuable molecules directly from air, turning an environmental challenge into a resource. Synthetic biology approaches enable the design of synthetic CO_2 fixation pathways never exhibited in nature. One example is the crotonyl-coenzyme A (CoA)/ethylmalonyl-CoA/hydroxybutyryl-CoA (CETCH) cycle, a synthetic CO_2 fixation pathway designed to operate faster and more efficient than the naturally evolved Calvin-Benson-Bassham cycle. The functionality of the CETCH cycle has been extensively validated through in vitro approaches. To advance toward biological implementation, we engineered *Pseudomonas putida* KT2440—a metabolically versatile, NADPH-rich chassis—to host modular CETCH components. To achieve this, we divided the CETCH pathway into four functional modules, expressing two on plasmids to test integration into native metabolism. Growth experiments revealed that strains expressing CETCH components exhibited enhanced growth on crotonate compared to control strains, particularly when methylmalonyl-CoA mutase activity was included. Through genetic engineering, we identified PP_3553 as a previously uncharacterized crotonyl-CoA ligase essential for crotonate metabolism in *P. putida*. To optimize flux through the CETCH pathway, we generated knockout strains (ΔFadB and ΔPP_3553) that eliminated native crotonate metabolism pathways. Metabolomics analyses showed limited carbon flux through the complete CETCH cycle, suggesting potential metabolic bottlenecks. Using auxotrophic sensor strains, we validated partial CETCH functionality and successfully evolved a strain with improved growth characteristics. This work demonstrates partial implementation of a synthetic carbon fixation pathway in *P. putida* and provides a foundation for future engineering efforts to develop more efficient biological carbon capture systems.

Acknowledgements

I would like to express my gratitude to Alberto Sánchez-Pascuala for his invaluable advice and supervision throughout this journey. Joseph Solomon, our conversations really helped shape my perspective on research and how I see the world. I am deeply appreciative of Beau Dronsella for his guidance on bacterial metabolism and for inspiring innovative solutions, particularly in navigating the complexities of metabolic networks when I faced challenges in my project. I extend my gratitude to the in-vivo subgroup, with special thanks to Hai He for his readiness to address my queries. To my friends Tobias Krug, Vaishnav Jadhav, Leo von Bank, Kevin Franzeck and Oyindrilla Samanta. I am immensely grateful for your unwavering support during the course of my thesis. I would like to express my profound appreciation to Tobi Erb. His leadership has taught me the importance of maintaining a broad perspective on scientific direction, managing a laboratory at a large scale, and effectively communicating ideas within the academic sphere. His example has shown me how to navigate the intricacies of academia. And last but not least, I want to thank my family for their unwavering support and love. They've been my rock throughout this journey, and I couldn't have done it without them.

Contributions

Contributor name	Contributor role
ASP, TJE, JSS	Conceptualization Ideas
ASP, JSS	Methodology
JSS, ASP, NP	Software
JSS	Validation
JSS, ASP, NP	Formal analysis
JSS, ASP, NP	Investigation
Erb lab, Metabolomic Core, Nikel lab	Resources
JSS	Data Curation
JSS	Writing - original draft preparation
JSS, ASP	Writing - review and editing
JSS, ASP	Visualization
ASP, TJE	Supervision
JSS, ASP	Project administration
TJE	Funding acquisition

JSS - Jogindh SS

ASP - Alberto Sánchez-Pascuala

TJE - Tobias J Erb

NP – Nicole Paczia

This contributor syntax is based on the Journal of Cell Science CRediT Taxonomy

1. Introduction

1.1 Rising Global Temperatures

Global warming has resulted in a temperature increase of 1.5°C above preindustrial levels, primarily driven by anthropogenic emissions of greenhouse gasses and aerosols (tiny particles) alongside natural emissions. Greenhouse gases in the atmosphere exhibit the capacity to absorb and re-emit infrared radiation, resulting in a net warming effect on Earth's surface. Conversely, aerosols predominantly scatter and reflect incoming solar radiation, thereby contributing to a cooling effect on the planet (Eltbaakh et al., 2012).

The primary driver of the rising temperatures is the emission of greenhouse gases, mainly carbon dioxide (CO_2), nitrous oxide and methane. Among these, CO_2 remains the largest contributor to global warming. Atmospheric carbon dioxide concentrations have risen from approximately 278 parts per million (ppm) in the mid-18th century to 480 ppm as of 2024, driven primarily by industrial-era fossil fuel emissions(*Emissions from Fossil Fuels Continue to Rise*, 2024). This human-induced surge has pushed CO_2 levels beyond the highest recorded concentrations in paleoclimate records spanning at least one million years (Fig. 1), with current accumulation rates exceeding any natural variability observed in the geological record(*Climate Change*, 2024; Lüthi et al., 2008).

The rise in global temperatures has contributed to an increased severity and frequency of heatwaves, as well as heightened intensity and volume of heavy precipitation and flooding (*AR6 Synthesis Report*, n.d.). Rising temperatures can also cause fluctuations in local climate leading to reduced crop yields, particularly in tropical regions. This issue is exacerbated by the growing global population, projected to reach 9.7 billion by 2050, which could lead to a food crisis. The increasing population also boosts energy demands, resulting in higher anthropogenic emissions.

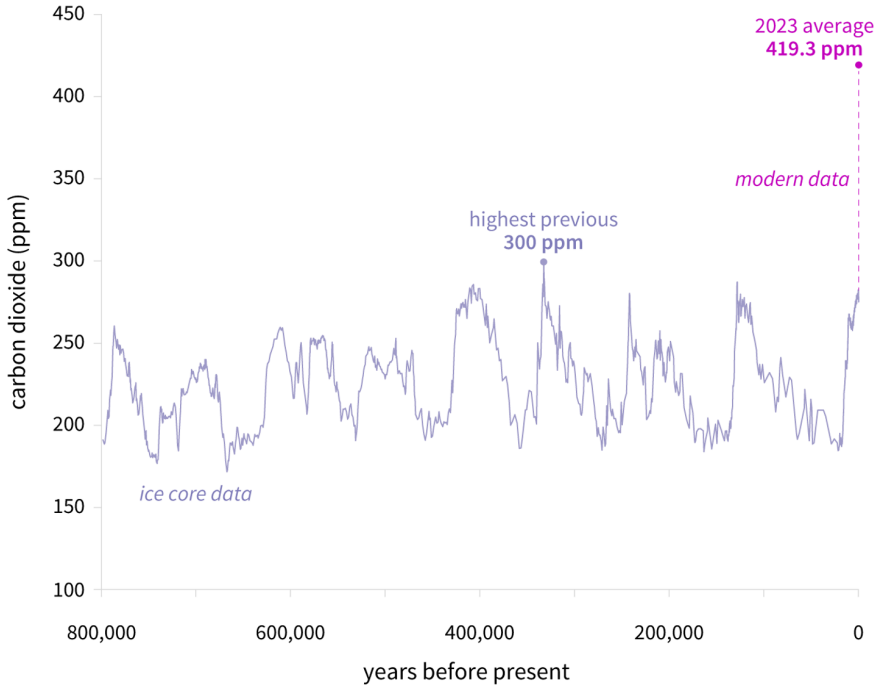

Figure 1) Atmospheric carbon dioxide (CO_2) concentrations over the past 800,000 years, based on ice-core data (light purple line), compared to the 2023 concentration (bright pink dot). The dashed pink line shows the increase over the past 60 years. Graph by NOAA.climate.gov. Data: (Lüthi et al., 2008)

Given the problem of rising CO_2 levels in the atmosphere, there are two potential solutions. One approach involves shifting anthropogenic energy emissions to more renewable sources; however, this does not address the damage accumulated over the years and may not be implementable quickly enough to meet rising energy demands. The other solution is to actively remove CO_2 from the atmosphere through carbon fixation.

1.2 Carbon fixation: Natural processes and Synthetic Opportunities

Carbon fixation, the process of converting inorganic carbon (primarily CO_2) into organic compounds, is fundamental to life on Earth. This process is challenging due to the thermodynamic stability of CO_2 and the significant energy input required for its conversion. The formation of carbon-carbon (C-C) bonds, a crucial step in carbon fixation, is particularly difficult due to the high activation energy required and the need for precise chemical control (Bar-Even et al., 2012).

Non-biological carbon fixation, such as industrial processes for CO_2 capture and conversion, accounts for only a small fraction of global carbon fixation. These processes often require harsh conditions, high energy inputs, and expensive catalysts, limiting their scalability and environmental sustainability (Liu et al., 2015).

Biological carbon fixation, on the other hand, dominates global CO_2 assimilation (Erb, 2024). Enzymes have evolved to overcome the thermodynamic and kinetic barriers associated with CO_2 utilization under mild physiological conditions. However, enzymatic carboxylation remains one of the most challenging biochemical reactions. The low atmospheric CO_2 concentration (~412 ppm) reduces substrate availability, driving equilibrium towards decarboxylation. Enzymes must precisely align CO_2 and acceptor substrates within their active sites while stabilizing reactive intermediates prone to side reactions. Furthermore, many carboxylases rely on energy-intensive cofactors (e.g., NADPH and ATP) or complex catalytic mechanisms to shift reaction equilibrium towards carboxylation (Erb, 2011).

Currently, autotrophic growth through photosynthesis by plants, cyanobacteria, algae and many other bacterial species plays the dominant role in absorbing atmospheric carbon dioxide. Through the process of photosynthesis, specifically the Calvin-Benson-Bassham (CBB) cycle, green plants on land remove and store an estimated 400 gigatons of CO_2 from the atmosphere each year(Erb, 2024). This makes land plants the most significant natural carbon sink on Earth. However, natural photosynthesis is insufficient to offset the rising anthropogenic CO_2 emissions.

The CBB cycle faces intrinsic limitations, primarily due to the characteristics of the enzyme RuBisCO (Ribulose-1,5-bisphosphate carboxylase/oxygenase). RuBisCO is relatively slow, fixing only 5–10 CO_2 molecules per second, whereas other key enzymes in carbon metabolism exhibit catalytic rates an order of magnitude higher(H et al., 2009; Sage, 2002). Additionally, RuBisCO the primary enzyme responsible for carbon fixation, exhibits a notable side-activity wherein it catalyzes the fixation of oxygen rather than CO_2. This oxygenation reaction yields 2-phosphoglycolate (2-PG), a toxic metabolite. The subsequent detoxification of 2-PG is an energy-demanding process. Moreover, this detoxification pathway, known as phosphoglycolate salvage pathway, results in a

substantial loss of fixed carbon, with up to 30% of previously assimilated carbon being released (Claassens et al., 2020; Xin et al., 2015).

This dual nature of RuBisCO's activity significantly affects the overall efficiency of carbon fixation in plants. Efforts to enhance the specificity and catalytic efficiency of RuBisCO through enzyme engineering have been pursued, but these modifications face trade-offs. Improvements in one aspect, such as catalytic speed, often result in reduced specificity, indicating that these factors are inherently linked(Erb, 2024). This interconnection has both has mechanistic and evolutionary reasons.

RuBisCO originated in an oxygen-free atmosphere prior to the first Great Oxygenation Event (~2.4 billion years ago). Initially, its function was unhindered by atmospheric oxygen (O_2). After the second Great Oxygenation Event (later Proterozoic Eon), rising O_2 levels forced RuBisCO to evolve enhanced specificity for CO_2 over O_2(Taylor-Kearney et al., 2024).

However, this adaptation came with a trade-off: improved discrimination against O_2 reduced its catalytic efficiency, making it slower at processing CO_2. Consequently, throughout its evolutionary history, RubisCO has been subject to a fundamental trade-off between catalytic efficiency and substrate specificity. This compromise remains a characteristic feature of all modern variants of the enzyme, with none having fully overcome this inherent limitation (Erb & Zarzycki, 2018). Alternatively, plants have also evolved alternative strategies to enhance carbon fixation efficiency. One such adaptation is the development of specialized compartments like pyrenoids, which function to concentrate CO_2 in the immediate vicinity of RuBisCO. This localized increase in CO_2 concentration effectively lowering the enzyme's oxygenase activity, thereby promoting more efficient carbon fixation and reducing the energetic costs associated with photorespiration(Kaste et al., 2024).

Since the discovery of the CBB, seven other naturally evolved pathways that revolve around other CO_2-fixing enzymes have been discovered(Santos Correa et al., 2023). The presence of these diverse pathways indicates that the range of potential CO_2-fixing enzymatic mechanisms is far more extensive than what has naturally evolved. This broader space includes pathways that are more efficient than those currently found in

nature (Schwander et al., 2016). However, evolutionary processes optimize for fitness, not solely for maximum carbon fixation efficiency, which explains why naturally evolved pathways may not represent the theoretical optimum. Consequently, the pathways that have evolved are only a small subset of what is theoretically possible and may be constrained by factors other than carbon fixation efficiency. In this context, synthetic biology provides a powerful tool for engineering and implementing novel CO_2 fixation pathways, where the primary optimization focus is on enhancing CO_2 capture. By designing such pathways rationally, scientists can explore a broader array of potential solutions to identify pathways with improved thermodynamic feasibility, faster kinetics, and reduced energy requirements.

1.3 Designing Synthetic Carbon Fixation Cycles

When designing synthetic carbon fixation pathways, several factors must be considered. The first is pathway kinetics, which addresses specific reaction bottlenecks, such as the speed of RuBisCO as discussed in previous sections. However, focusing solely on kinetics is insufficient, as it does not account for thermodynamic factors such as the energy cost of the pathway. To evaluate this, one must consider feasibility, which can be assessed through the consumption of reducing equivalents (e.g., NADPH, ferredoxins, NADH, $FADH_2$, or other redox carriers) or energy carriers like ATP and ATP equivalents (e.g., NTPs and CoAs). These parameters are used to calculate the overall free energy of the pathway, which determines its thermodynamic feasibility. For a reaction to proceed spontaneously, the free energy must be negative(Bar-Even et al., 2010).

Thermodynamic feasibility and energy efficiency often present a delicate balance in pathway design. As the energy consumption of a pathway increases to ensure thermodynamic favorability, its overall energy efficiency tends to decrease. This inverse relationship highlights a crucial trade-off:

Pathways that are more thermodynamically favorable (i.e., have a more negative free energy change) typically require a higher energy input, which in turn reduces their net energy efficiency. Conversely, highly energy-efficient pathways may operate closer to

thermodynamic equilibrium, potentially compromising their robustness or rate of product formation(Schulz-Mirbach et al., 2024).

This trade-off underscores the importance of optimizing both thermodynamic feasibility and energy efficiency in the design of synthetic metabolic pathways, particularly for carbon fixation processes where energy conservation is paramount(Bar-Even et al., 2010).

Another crucial consideration is topological compatibility. This involves assessing the number of enzymes required in the synthetic pathway and their integration into the native metabolic network of the host organism. It is essential to ensure that these enzymes do not disrupt native pathways critical for survival or interfere with essential cellular functions(Bar-Even et al., 2010).

1.4 The CETCH (crotonyl-CoA/ethylmalonyl-CoA/hydroxybutyryl-CoA) Cycle

As previously discussed, a significant limitation of carbon fixation pathways is often the efficiency of the carboxylating enzyme. Within this context, a recently discovered class of enzymes, the Enoyl-CoA Reductases/Carboxylases (ECRs), has emerged as a promising biotechnological candidate. Initially identified in alpha proteobacteria, ECRs have multiple possible activities. These enzymes can catalyze the reduction of enoyl-CoA to saturated acyl-CoA or perform the reductive carboxylation of α,β-unsaturated enoyl-CoAs . They utilize NADPH as an electron donor to drive the energetically demanding CO_2 fixation step(Erb et al., 2009). Notably, ECRs exhibit remarkable catalytic efficiency, with a turnover (kcat) of 100 s^{-1}, significantly outperforming traditional carbon-fixing enzymes such as RuBisCO(Cotton et al., 2018; Schwander et al., 2016).

The medium-chain dehydrogenase/reductase (MDR) superfamily, to which ECRs belongs, inherently possesses the capacity to interact with CO_2. Through evolutionary processes, ECRs have acquired four highly conserved residues—Asn81, Phe170, Glu171, and His365—that play essential roles in favoring carboxylation over the ancestral reductive function. This adaptive shift has enabled these enzymes to achieve efficient

CO_2 fixation, representing a metabolic innovation. The emergence and conservation of these specific residues underscore the molecular basis for the functional divergence from simple reduction to carboxylation within this enzyme family (Bernhardsgrütter et al., 2019; Erb et al., 2009).

Among the ECRs, crotonyl-CoA carboxylase/reductase (Ccr) stands out as a particularly efficient CO_2-fixing enzyme. Ccr catalyzes the NADPH-dependent reductive carboxylation of crotonyl-CoA to ethylmalonyl-CoA. This remarkable catalytic efficiency makes Ccr one of the fastest known CO_2-converting enzymes, surpassing the average RuBisCO homolog by nearly an order of magnitude.

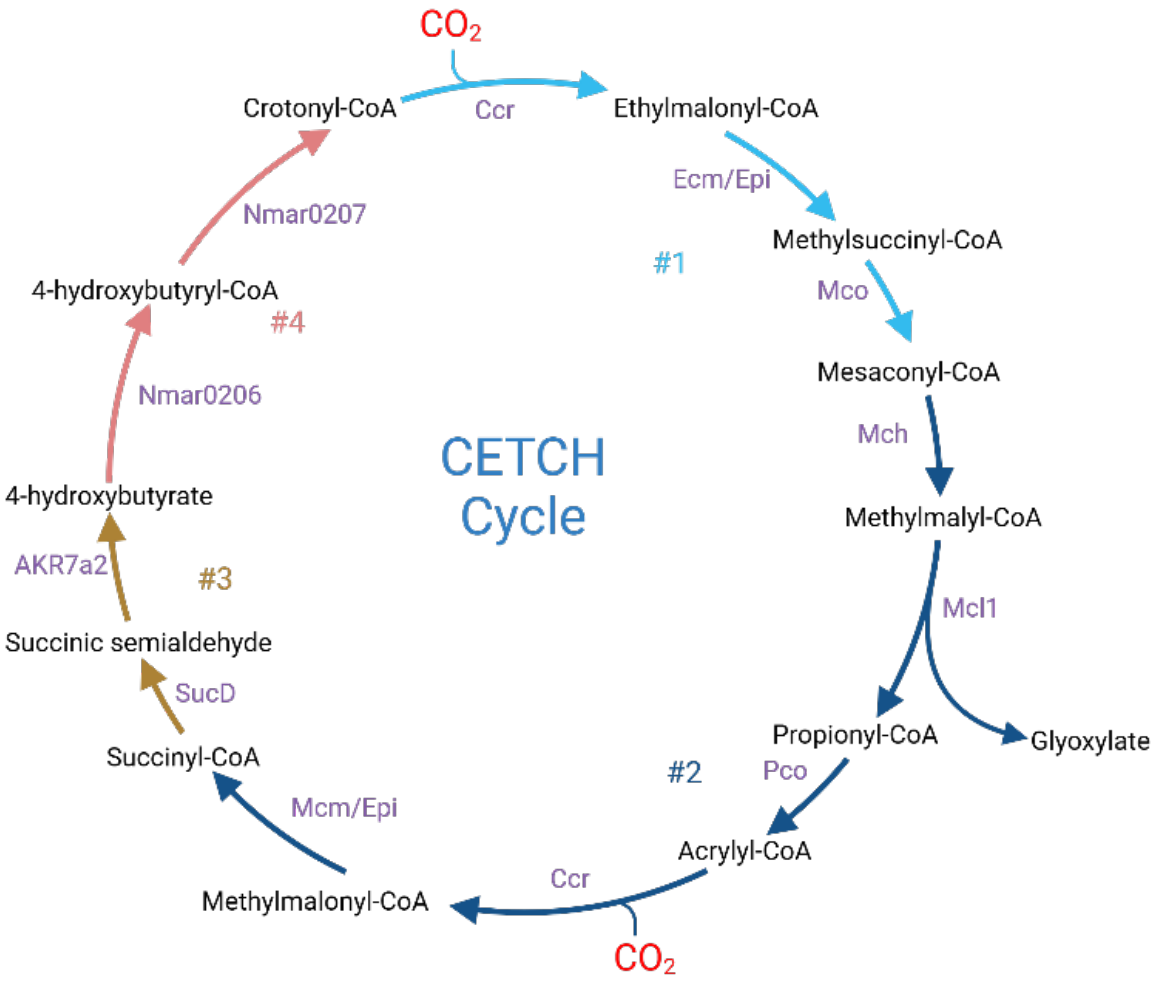

Figure 2) CETCH (crotonyl-CoA/ethylmalonyl-CoA/hydroxybutyryl-CoA) cycle scheme depicting the four different modules in different colours. Adapted from Sánchez-Pascuala et al. in preparation; Numbers

represent independent modules for implementation. Enzymes in light purple. Ccr: Crotonyl CoA Carboxylase; Ecm/Epi: Methyl-malonyl CoA – Ethyl-malonyl CoA/Epimerase; Mco: Methyl-succinyl CoA oxidase; Mesaconyl CoA hydratase; Mcl1: β methyl malyl CoA lyase; Pco: Propionyl CoA Oxidase; SucD: Succinate CoA lyase; AKR7a2: Aldo-Keto Reductase Family 7 Member A2; Nmar0206*: Nitrosopumilus maritimus* 4-hydroxybutyryl-CoA synthetase; Nmar0207*: Nitrosopumilus maritimus* 4-hydroxybutyryl-CoA dehydratase

Building around Ccr one possible synthetic pathway is the CETCH cycle (crotonyl-CoA/ethylmalonyl-CoA/hydroxybutyryl-CoA). It is a rationally designed synthetic carbon fixation pathway that merges two natural metabolic modules: the 3-hydroxypropionate/4-hydroxybutyrate (3HP/4HB) cycle, renowned for its high ATP efficiency in aerobic CO_2 fixation, and the ethylmalonyl-CoA (EMC) pathway, which enables acetate assimilation via glyoxylate regeneration(Erb et al., 2007; Loder et al., 2016).

The CETCH cycle is a synthetic carbon fixation platform comprising 12 core reactions (Fig. 2), done by enzymes assembled from organisms across all three domains of life, optimized for catalytic efficiency. A key innovation includes the *de novo* creation of methyl succinyl-CoA oxidase, engineered through rational redesign of methyl succinyl-CoA dehydrogenase. Central to its function are two NADPH-dependent carboxylation steps (Fig. 3A) catalyzed by crotonyl-CoA carboxylase/reductase (Ccr). Comparative analyses reveal the CETCH cycle operates with 20% lower energy demand than the Calvin-Benson-Bassham (CBB) cycle (Fig. 3B), achieved through kinetic and thermodynamic optimizations. The CETCH has recently been engineered to show functional CO_2 fixation *in vitro*, while computational modeling—using enzyme cost minimization algorithms and thermodynamic constraints—has predicted superior product-substrate yields(Löwe & Kremling, 2021; Schwander et al., 2016). The cycle's thermodynamic favorability arises from tight coupling of exergonic (e.g., ATP hydrolysis) and endergonic reactions, minimizing energy dissipation through electron loss. With the pathway now functional, in vitro the next step would be to evaluate its transplantation into a living cell for efficient scale-up of the reactions.

Whole-cell biocatalysis presents several key advantages over using purified enzymes in biotechnological processes. This approach significantly reduces production costs by eliminating the need for enzyme purification steps. Additionally, the cellular environment

naturally supports cofactor regeneration, enhancing overall reaction efficiency. Enzymes within whole cells benefit from increased stability and protection against external factors, leading to improved catalytic performance. Furthermore, the inherent compartmentalization of cellular structures allows for better control and efficiency of multiple reactions occurring simultaneously. These combined benefits make whole-cell biocatalysis an attractive and often more practical option for various industrial and research applications, offering a more economical and robust alternative to traditional purified enzyme systems.

A

CETCH cycle: $2\ CO_2 + 3\ NAD(P)H + 2\ ATP + FAD \rightarrow glyoxylate + 3\ NAD(P)^+ + 2\ ADP + 2\ P_i + FADH_2$

CBB cycle: $3\ CO_2 + 6\ NAD(P)H + 9\ ATP \rightarrow 3\text{-}phosphoglyceraldehyde + 6\ NAD(P)^+ + 9\ ADP + 9\ P_i$

B

Parameter	CETCH	CBB
Primary CO_2 Fixation product	Glyoxylate	Glyceraldehyde-3 P
Net NADPH consumption	9	7
Net ATP consumption	3	12
ATP equivalent per CO_2 Fixed	6.5	9.9

Figure 3) A) Comparison between reactions of the CBB and the CETCH. B) Comparison of the energetics of CBB and the CETCH

1.5 *Pseudomonas putida* KT2440: A promising candidate for CETCH implementation

One possible candidate for *in-vivo* implementation is the gram-negative saprophytic soil bacterium strain *Pseudomonas putida* KT2440. The strain traces its origins to the isolation of *P. putida* mt-2 (initially named *Pseudomonas arvilla* mt-2) from soil in a Japanese field in 1963(Nakazawa, 2003). This parent strain possessed a toluene-degrading TOL plasmid, enabling it to metabolize aromatic hydrocarbons. In the 1980s, researchers genetically modified mt-2 to create KT2440 by curing the TOL plasmid. Following this in 2014, chromosomal restriction systems and prophages were disabled, resulting in a safer and more genetically tractable strain(Martínez-García et al., 2014).

These changes allowed easier DNA manipulation while retaining environmental survival capabilities(de Lorenzo et al., 2024).

This bacterium is increasingly used for industrial and environmental biotechnology because of its ability to withstand oxidative stress while being non-pathogenic. It can also rapidly grow and has versatile metabolism, along with the availability of molecular tools for advanced genetic programming.

The metabolic architecture of *P. putida* provides it with several advantages when it comes to redox status. The bacterium lacks the enzyme phosphofructokinase (Pfk) causing it to not metabolize glucose through the Embden-Meyerhof-Parnas (EMP) pathway(Chavarría et al., 2013). Alternatively, glucose is assimilated via phosphorylation by glucokinase or oxidation to gluconate or 2-ketogluconate. Both these pathways then converge to 6-phosphogluconate which then enters into the Entner Duodoroff (ED) pathway. The combination of enzymes from ED pathway, pentose phosphate pathway and partial EMP pathway together produce the EDEMP cycle. This architecture allows triose phosphate recycling through the gluconeogenic EMP reactions, thus allowing it to produce reducing power based on the environmental circumstances(Nikel et al., 2015). By favoring the ED pathway over glycolysis, *P. putida* sacrifices an ATP per glucose molecule but gains a NADPH – an evolutionary adaptation enhancing environmental resilience for oxidative stress tolerance, minimized protein burden and utilization of more varied carbon sources (Flamholz et al., 2013; Stettner & Segrè, 2013). This NADPH-rich metabolism aligns with biotechnological applications like powering the CETCH cycle, which requires substantial reducing power (NADPH) to drive CO_2 fixation (Fig. 4C). The metabolic structure is also versatile as shown by the implementation of the complete linear glycolysis in the bacterium(Sánchez-Pascuala et al., 2019).

P. putida also has the Polyhydroxyalkanoate (PHA) cycle. This pathway acts as a metabolic capacitor, dynamically balancing fluxes of carbon and electrons to maintain homeostasis during metabolic perturbations. Thus, energy intensive pathway implementation this cycle can act as a metabolic buffer (Manoli et al., n.d.). It is indeed promising that *P. putida* is a suitable candidate for the CETCH pathway, as the

ethylmalonyl-CoA pathway has already been partially implemented in this strain and is a component of the CETCH cycle (Gross et al., 2006).

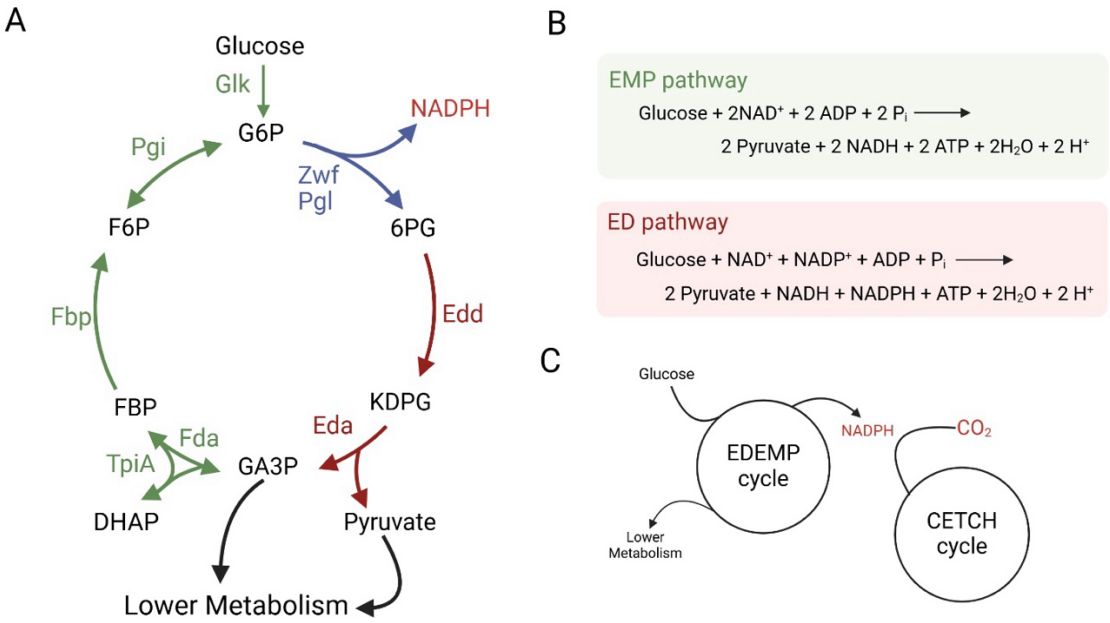

Figure 4 A) Schematic representation of glucose catabolism in *P. putida* KT2440, highlighting the predominant Entner-Doudoroff (ED) pathway (red). The majority of glucose enters central carbon metabolism as 6-phosphogluconate, which is then channeled through the ED pathway. A portion of glucose 6-phosphate is directed through the pentose phosphate pathway (purple), converging with the ED pathway at 6-phosphogluconate. Notably, some of the generated triose phosphates undergo recycling to form hexose phosphates via gluconeogenesis through the partial Embden-Meyerhof-Parnas (EMP) pathway (green). B) Comparative analysis of the EMP and ED pathways. The ED pathway yields one less ATP molecule per glucose molecule compared to the EMP pathway. The ED pathway produces a net yield of 1 ATP, 1 NADH, and 1 NADPH per glucose molecule, while the EMP pathway generates 2 ATP and 2 NADH molecules. C) Proposed strategy for harnessing the NADPH surplus generated through the EDEMP cycle for carbon fixation via the CETCH cycle. Glk: Glucokinase; Zwf: Glucose-6-phosphate dehydrogenase; Pgl: Phosphogluconolactonase; Edd: Phosphogluconate dehydratase; Eda: Aldolase; Fda: Fructose 1,6 - bisphosphate aldolase; TpiA: Triosephosphate isomerase; Fbp: Fructose 1,6 – bisphosphatase; Pgi: Glucose-6-phosphate isomerase. G6P: Glucose-6-phosphate; P_i: Inorganic phosphate; 6PG: 6-Phosphogluconate; KDPG: 2-Keto-3-deoxy-6-phosphogluconate; GA3P: Glyceraldehyde-3-phosphate; DHAP: Dihydroxyacetone phosphate; F6P: Fructose-6-phosphate.

1.6 Aim of This Work

The aim of This Work was to evaluate the potential of *P. putida* KT2440 as a host for the CETCH cycle and to engineer the strain for the expression of functional modules of the pathway. With this goal, we employed two strategies in This Work to implement a synthetic pathway into our model organism of interest.

The first was to express genes of the pathway directly in a wild-type strain and then remove peripheral pathways that seep out metabolic flux from our pathway of interest by making targeted deletions. This way we could rapidly establish a functional prototype. Consequently, we could quickly identify metabolic bottlenecks for iterative engineering. We can also leverage the native robustness and stress resistant abilities of the wild-type strain while implementing pathways with toxic intermediates.

The second strategy was to couple growth of the model organism to pathway activity via auxotrophic engineering. For this there needs to first be a rationally designed selection strain, which has strategic deletions that prevents growth in certain media conditions (Fig. 5A). When no pathway is present, the auxotrophy is relieved by supplementation of a particular essential metabolite. The pathway of interest would then relieve the auxotrophy thus allowing the strain to grow in selective conditions (Fig 5B). Maintaining the selective pressure can also then be used to evolve the strain through a process called Adaptive Laboratory Evolution (ALE).

The dual top-down and bottom-up approach provided a systematic framework for engineering *P. putida* KT2440 and allowed us to flexibly explore various possibilities for pathway implementation.

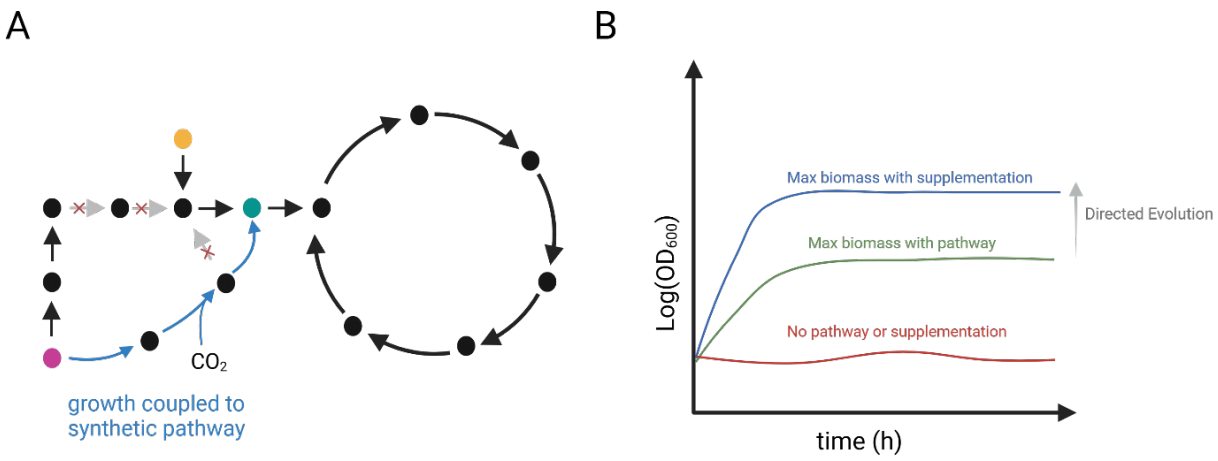

Figure 5) A) The metabolic network depicts an auxotrophic strain that exhibits selective growth on a specific carbon source (pink) while maintaining the ability to grow on an alternative carbon source (yellow). Black dots represent essential biomass precursors. The green molecule indicates the compound for which the strain is auxotrophic. Grey arrows with crosses represent gene deletions. A synthetic carbon fixation pathway (blue) is integrated into the network, coupled to the formation of an essential metabolite under selective conditions. B) Successful operation of the synthetic pathway enables growth under selective conditions, providing a foundation for directed evolution. This approach can be leveraged to enhance growth rate and increase overall biomass production. Figure adapted from (Orsi et al., 2021)

2. Material and Methods

2.1 Primer list

Table of DNA oligo primers used in This Work:

Oligos were ordered from Eurofins Genomics, Anzinger Straße 7a, D-85560 Ebersburg and Sigma-Aldrich Chemie GmBH, Eschenstrasse 5, 82024, Taurfkirchen bei Muenchen.

Primer Name	**Primer Sequence**	**Purpose**	**Source**
Amplification_Gibson_F_PccBA_Mcm	GCGCGAATTCGAGCTCAG	Gibson Cloning of PccB, PccA CETCH variant	This Work
Amplification_Gibson_R_PccBA_Mcm	CCTCCTCCCGGGTACCTTATG	Gibson Cloning of PccB, PccA CETCH variant	This Work
F-SacI-PccBA-Mcm	CGAGCTCAGGAGGAAAAACATATGAAAGATATCCTTGAAAAAC	Restriction Cloning of PccB, PccA CETCH variant	This Work
R-KpnI-PccBA-Mcm	CGGGTACCTTATGAGCGAGCCTCACGAATC	Restriction Cloning of PccB, PccA CETCH variant	This Work
JS2,3_mcm_mch_verification_F	GTTGGCATTTCCAGTTTAGC	Verification of PccB, PccA CETCH variant plasmid	This Work
JS2,3_mcm_mch_verification_R	GCATAACCTAAATTGGCCAC	Verification of PccB, PccA CETCH variant plasmid	This Work
JS1_mcm_pco_verification_F	TGTCATGGTTGCCTGGCAAC	Verification of Pco CETCH variant plasmid	This Work
JS1_mcm_pco_verification_R	TCAGGCGATTTGCCTTTGAG	Verification of Pco CETCH variant plasmid	This Work
F_ppk_Pputida	GTTTCCCGCGCGATCATGTC	Verification of *P. putida* KT2440 strain	This Work
R_ppk_Pputida	GCTTCAAGACCCACGCCAAG	Verification of *P. putida* KT2440 strain	This Work
TS1_F_PP_3553	GGAATTCCGCCATGGCGCTCTTCACTG	Amplification of flanking regions of PP_3553 for knockout plasmid	This Work
TS1_R_PP_3553	GAAGGGGAGCGGCTATGGCAGCGGTAATCCTGTAAGGGAG	Amplification of flanking regions of PP_3553 for knockout plasmid	This Work

TS2_F_PP_3553	TGCCATAGCCGCTCCCCTTC	Amplification of flanking regions of PP_3553 for knockout plasmid	This Work
TS2_R_PP_3553	CGGGATCCGCAGCTGCCTGCG CTCAATG	Amplification of flanking regions of PP_3553 for knockout plasmid	This Work
Check_F_PP_3553	CAGGTCATCGTGTGGTAGCC	External primers for verification of ΔPP_3553 strain	This Work
Check_R_PP_3553	CATCCGGCATTTTGGCCAGC	External primers for verification of ΔPP_3553 strain	This Work
TS1F_PP_2136	GGAATTCCATCCAGGCTGGTC AATCTG	Amplification of flanking regions of PP_2136 for knockout plasmid	This Work
TS1R_PP_2136	CGCTCTAGCTCGTTGACCGCC AACTGATCTCCACGATATG	Amplification of flanking regions of PP_2136 for knockout plasmid	This Work
TS2F_PP_2136	GCGGTCAACGAGCTAGAGCG	Amplification of flanking regions of PP_2136 for knockout plasmid	This Work
TS2R_PP_2136	TGGGCCTGACTGCAGAAATGG GATCCCG	Amplification of flanking regions of PP_2136 for knockout plasmid	This Work
TS1F_FadBAq-EcoRI	GGAATTCCCATCGAGCAGATG ATGGCC	Amplification of flanking regions of PP_2136 for truncated knockout plasmid	This Work
TS1F_FadBAq	CCCATGATTGCCGGGTCGACA TTGGCGAAATCGCCATAGG	Amplification of flanking regions of PP_2136 for truncated knockout plasmid	This Work
TS1F_FadBAq	GTCGACCCGGCAATCATGGG	Amplification of flanking regions of PP_2136 for truncated knockout plasmid	This Work
TS1F_FadBAq-BamHI	CGGGATCCCTTCGGTTTCGGA GTGCCGC	Amplification of flanking regions of PP_2136 for truncated knockout plasmid	This Work
Check_F_PP_2136	CGGCCATAGAATCTCCTACG	External primers for verification of ΔFadB strain	This Work
Check_R_PP_2136	CAAGTCTTTCAGCACGGGCAG	External primers for verification of ΔFadB strain	This Work
TS1F_PP_2217	GAATTCCGCCAGCACGCCTCC GACACC	Amplification of flanking regions of PP_2217 for knockout plasmid	This Work
TS1R_PP_2217	GGCATTGTCCGCAGCGAGGAG CAGTCTGCTCCTTCAAAGA	Amplification of flanking regions of PP_2217 for knockout plasmid	This Work
TS2F_PP_2217	TCCTCGCTGCGGACAATGCC	Amplification of flanking regions of PP_2217 for knockout plasmid	This Work
TS2R_PP_2217	CGGATCCGACGGCAACGAACC GAGTCTG	Amplification of flanking regions of PP_2217 for knockout plasmid	This Work

prpC_v2_TS1F	GGAATTCCTGCCGTCGACGCCCGCAGCG	Amplification of flanking regions of prpC for knockout plasmid	This Work
prpC_v2_TS1R	TTCAAGAAAGGAGAAACACCATAGCTATAGAGAGGCAACC	Amplification of flanking regions of prpC for knockout plasmid	This Work
prpC_v2_TS2F	ATAGCTATAGAGAGGCAACC	Amplification of flanking regions of prpC for knockout plasmid	This Work
prpC_v2_TS2R	CGGATCCGGGTCGACGATCAGTTGCACC	Amplification of flanking regions of prpC for knockout plasmid	This Work
TS1F_prpC_from_pSMW2	CTGAATTCGAGCTCGGTACC	Cloning out prpC flanking regions from prpC_pSNW2 plasmid	This Work
TS2R_prpC_from_pSMW2	CGGGATCCGTGGTCGACGATCAGTTGCAC	Cloning out prpC flanking regions from prpC_pSNW2 plasmid	This Work
Check_prpC_P.putida_F	TTCAAGGCCATCTACCTGTC	External primers for verification of ΔPrpC strain	This Work
Check_prpC_P.putida_R	ACCCAGTGCATCGACATGCG	External primers for verification of ΔPrpC strain	This Work

2.2 Table of plasmids used in this work

Abbreviation	Name	Source
pS224	pSEVA224	Lab collection
pS438	pSEVA438	Lab collection
pASPASP93	pSEVA438-Mch-Mcl1-PA4198	Sánchez-Pascuala et al. in preparation
pASP212	pSEVA224-Ccr-Ecm-Epi-Mco	Sánchez-Pascuala et al. in preparation
pASPASP224	pSEVA224-Mch-Mcl1-Nmar0206-Nmar0207-SucD-AKR7a2	Sánchez-Pascuala et al. in preparation
pASP237	pSEVA224-PccB-PccA-Mcm	Sánchez-Pascuala et al. in preparation
pASP234	pSEVA224-Ccr-Ecm-Epi-Mco-Pco	Sánchez-Pascuala et al. in preparation
JS1	pSEVA224-Ccr-Ecm-Epi-Mco-Pco-Mcm	This Work
pMcmControl	pSEVA224 - Mcm	This Work
pPA4198Control	pSEVA224 – PA4198	This Work
pEMG	pEMG	(Martínez-García et al., 2023)
pSW1	pSW1	(Martínez-García et al., 2023)
pSNW2	pSNW2	(Volke et al., 2020)
pGNW2	pGNW2	(Volke et al., 2020)
pQURE-6H	pQURE-6H	(Volke et al., 2020)

pSNW2 - PP_2217	pSNW2 - PP_2217 flanking regions	This Work
pSNW2 - PP_2136	pSNW2 - PP_2136 flanking regions	This Work
pSNW2-prpC_1	pSNW2-prpC_1 flanking regions	This Work
pSNW2-prpC_2	pSNW2-prpC_2 flanking regions	This Work
pEMG-prpC_2	pEMG-prpC_2 flanking regions	This Work
pEMG-FadBtrunc	pEMG-FadBtrunc flanking regions	This Work

2.3 Table of strains used in This Work

Strain Name	**Genotype**	**Source**
CETCH(-)	*P. putida* KT2440 + pSEVA224 + pSEVA438	This Work
CETCH(1)(2)(-mcm)	*P. putida* KT2440 + pASPASP93 + pASP212	This Work
E. coli DH5α	*F−λ− Φ80lacZΔM15 Δ(lacZYA-argF)U169 deoR recA1 endA1 hsdR17(rK− mK+) phoA supE44 thi-1 gyrA96 relA1*	Lab Collection
DH5α pSEVA224	*E. coli* DH5α + pSEVA224	This Work
DH5α pASP237	*E. coli* DH5α + pASP237	This Work
DH5α pASPASP93	*E. coli* DH5α + pASPASP93	This Work
DH5α pSEVA438	*E. coli* DH5α + pSEVA438	This Work
DH5α pASPASP224	*E. coli* DH5α + pASP224	This Work
P. putida KT2440 WT	*P. putida* KT2440	This Work
CETCH(1)(2)(+mcm)	*P. putida* KT2440 + pASP93 + JS1	This Work
E. coli DH5α *λpir*	*E. coli* DH5α *sup E44, ΔlacU169 (ΦlacZΔM15), recA1, endA1, hsdR17, thi-1, gyrA96, relA1, λpir*	Lab Collection
pSNW2 DH5α *λpir*	*E. coli* DH5α *λpir* + pSNW2	(Volke et al., 2020)
DH5α pQURE6H	*E. coli* DH5α + pQURE6H	(Volke et al., 2020)
DH5α mcm Control	*E. coli* DH5α + pMcmControl	This Work
PP_3553 DH5α *λpir*	*E. coli* DH5α *λpir* + pSNW2 - PP_3553	This Work
P. putida PP_3553 coint	*P. putida* KT2440 :: pSNW2 - PP_3553	This Work
P. putida PrpC coint	*P. putida* KT2440 :: pSNW2 - PrpC	This Work
P. putida mcm Control	*P. putida* KT2440 + pMcmControl + pS438	This Work
P. putida PA4198 Control	*P. putida* KT2440 + pPA4198Control + pS438	This Work
P. putida FadB coint	*P. putida* KT2440 :: pSNW2 – PP_2136	This Work
DH5α - pEMG	*E. coli* DH5α *λpir* + pEMG	This Work

DH5α – pSW1	*E. coli* DH5α *λpir* + pSW1	This Work
P. putida ΔFadB	*P. putida* KT2440 ΔFadB	This Work
P. putida ΔPP_3553	*P. putida* KT2440 *ΔPP_3553*	This Work
P. putida ΔPP_3553 EV	*P. putida* KT2440 *ΔPP_3553* + pS224 + pS438	This Work
P. putida ΔPP_3553 CETCH	*P. putida* KT2440 Δ*PP_3553* + pASP93 + JS1	This Work
P. putida ΔFadB EV	*P. putida* KT2440 ΔFadB + pASP93 + JS1	This Work
P. putida ΔFadB CETCH	*P. putida* KT2440 ΔFadB + pS224 + pS438	This Work
P. putida ΔPP_3553 PA4198	*P. putida* KT2440 Δ*PP_3553* + pPA4198Control + pS438	This Work
P. putida Suc CoA Aux	*P. putida* SEM11 Δ*SucABCD* Δ*AceA* Δ*ScpC* Δ*AspC*	Nikel lab
P. putida Gly Aux	*P. putida* EM42 Δ*SerA* Δ*ltaE* Δ*AceA*	Nikel lab
P. putida Gly Aux CETCH	*P. putida* EM42 Δ*SerA* Δ*ltaE* Δ*AceA* + pASP93 + JS1	This Work
P. putida Suc CoA Aux CETCH	*P. putida* SEM11 Δ*SucABCD* Δ*AceA* Δ*ScpC* Δ*AspC* + pASP93 + JS1	This Work
P. putida ΔFadB ΔPP_3553	*P. putida* KT2440 ΔFadB Δ*PP_3553*	This Work
P. putida Gly Aux EV	*P. putida* EM42 Δ*SerA* Δ*ltaE* Δ*AceA* + pS224 + pS438	This Work
P. putida Suc CoA Aux EV	*P. putida* SEM11 Δ*SucABCD* Δ*AceA* Δ*ScpC* Δ*AspC* + pS224 + pS438	This Work
P. putida ΔFadB ΔPP_3553 EV	*P. putida* KT2440 ΔFadB *ΔPP_3553* + pASP93 + JS1	This Work
P. putida ΔFadB ΔPP_3553 CETCH	*P. putida* KT2440 ΔFadB *ΔPP_3553* + pS224 + pS438	This Work
P. putida Suc CoA Aux CETCH Evo_1	*P. putida* SEM11 *ΔSucABCD ΔAceA ΔScpC ΔAspC* + pASP93 + JS1 [Evolved]	This Work

2.4 Chemicals

SIGMA-ALDRICH	St. Louis, USA
THERMO FISHER SCIENTIFIC	Waltham, USA
MERCK	Buchs, Switzerland
CARL-ROTH	Karlsruhe
EVONIK	Essen
FLUKA	Darmstadt, Germany

2.5 Kits

Monarch ® Plasmid Miniprep Kit, NEB Ipswich, USA

Monarch ® Nucleic Acid Purification Kit, NEB
Ipswich, USA

Monarch ® DNA Gel Extraction Kit, NEB Ipswich, USA

2.6 Media, buffers and solutions

LB medium

0.5 % (w/v) Yeast extract

1.0 % (w/v) NaCl

1.0 % (w/v) Peptone/tryptone

LB Agar

0.5 % (w/v) Yeast extract

1.0 % (w/v) NaCl

1.0 % (w/v) Peptone/tryptone

1.5 % (w/v) Agar

(5X) M9 Salts

64 g Na_2HPO_4 . 7H2O

15 g KH_2PO4

2.5 g NaCl

5 g NH_4Cl

1 L H_2O

M9 Minimal Media

800 µl 1M MgSO4

80 ml (5x) M9 Salts

40 µl 1M $CaCl_2$

4 ml Trace metals

400 µl Fe solution

Up to 400 ml H_2O

Gentamycin stock solution

50 mg/ml in ddH_2O, stored at – 20 °C

Kanamycin stock solution

50 mg/ml in ddH_2O, stored at – 20 °C

Spectinomycin stock solution

50 mg/ml in ddH_2O, stored at – 20 °C

Ampicillin stick solution

100 mg/ml in ddH_2O, stored at – 20 °C

300 mM Sucrose

102.68 g of Sucrose in 1L H2O

Carbon Sources

1M Glucose

180.16 g of Glucose in 1L H_2O

400 mM Crotonate

42.392 g of Sodium Crotonate in 1L H_2O

500 mM Succinate

81.025 g of Sodium Succinate in 1L H_2O

1M Glyoxylate

96.2 g of Sodium Glyoxylate in 1L H_2O

1M Formate

68 g of Sodium Formate in 1L H_2O

1M Propionate

96.07 g of Sodium Propionate in 1L H_2O

2.5 Software

Benchling	© BENCHLING
GraphPad Prism	© DOTMATICS
Geneious Prime	© DOTMATICS
MS Office Professional 2016	© Microsoft Corporation
PyMol	© Schrödinger

2.6 Online Databases/Softwares

EcoCyc	SRI International
BioCyc	SRI International
Pseudomonas Genome DB	Cystic Fibrosis Foundation
BLAST	National Institute of Health
Alphafold	Google DeepMind
Uniprot	Uniprot Consortium

2.7 Methodology

2.7.1 Culture conditions of bacterial strains

E. coli strains were cultured overnight in Luria-Bertani (LB) medium supplemented with appropriate antibiotics (kanamycin 50 µg/mL, spectinomycin 50 µg/mL, or gentamicin 20 µg/mL) at 37°C with shaking at 150 rpm. *P. putida* strains were grown either overnight or for two days, depending on the strain, in either LB medium or M9 minimal medium supplemented with 20 mM glucose. *P. putida* cultures were incubated at 30°C with shaking at 150 rpm.

2.7.2 Growth phenotype measurements

To analyze the growth phenotype continuously, a microplate reader (Biotek Synergy H1 Microplate Reader) was utilized. *P. putida* strains were first inoculated in 10 mL of M9 minimal media supplemented with 20 mM glucose and cultured until they reached the stationary phase. The cells were then harvested by centrifugation at 4000g for 10 minutes. Following centrifugation, the cell pellets were washed twice with M9 media lacking glucose to remove residual carbon sources and resuspended in 1× M9 media without any carbon source.

The optical density at 600 nm (OD600) of the washed cells was measured, and the volume required for each well was calculated by normalizing the OD_{600} to 0.05. A calculated volume of the cell suspension was then mixed with 150 µL of respective media in inducing conditions (0.5 mM Isopropyl β-D-1-thiogalactopyranoside, 0.5 mM 3-methyl benzoate, 50 µg/ml kanamycin, 80 µg/ml spectinomycin, 1 µg/ml biotin, 1 µM vitamin B_{12}) and pipetted into individual wells of a 96-well Nunclon plate (Thermo Fisher Scientific). To prevent contamination while allowing gas exchange, 50 µL of mineral oil was added on top of each well. The prepared plate was placed into the microplate reader, which was set to maintain a controlled environment with 5% CO_2, a temperature of 30°C, and continuous agitation during the experiment.

2.7.3 Construction of CETCH module vectors

Plasmids were designed and constructed in silico using Geneious Prime software, employing either Gibson assembly or restriction digestion methods. For Gibson

assembly, the software was used to design appropriate overlapping sequences for joining of multiple DNA fragments. For restriction digestion, the software's restriction cloning tool was utilized to select appropriate restriction sites and simulate the cloning process.

2.7.4 Polymerase Chain Reaction (PCR) composition for amplifying DNA fragments for Gibson assembly

The backbone and gene fragments were amplified from two sources: vectors previously constructed by Dr. Alberto Sánchez-Pascuala at the Max Planck Institute for Terrestrial Microbiology (MPI-TM), and *P. putida* KT2440 genomic DNA. Polymerase Chain Reaction (PCR) was used to amplify these DNA segments. The resulting PCR products were then used for subsequent cloning steps, such as ligation or assembly into the final construct.

Reaction Setup:

Component	**25 µl Reaction**
Q5 High-Fidelity 2X Master Mix	12.5 µl
10 µM Forward Primer	1.25 µl
10 µM Reverse Primer	1.25 µl
Template DNA	Variable (< 1,000 ng)
Nuclease-Free Water	To 25 µl

Thermal Cycler Program:

Step	**Temp**	**Time**
Initial Denaturation	98°C	30 seconds
25–35 Cycles	98°C	5–10 seconds
	*50–72°C	10–30 seconds
	72°C	20–30 seconds/kb
Final Extension	72°C	2 minutes

Hold	4–10°C	

*NEB T_m calculator was used temperature

2.7.5 Agarose Gel Electrophoresis:

Agarose gel electrophoresis was performed using a 0.8% (w/v) agarose gel prepared by dissolving 0.8 g of agarose powder in 100 mL of buffer. GeneRuler 1 kb Plus DNA Ladder was used as a molecular weight standard. The gel was subjected to electrophoresis at 100 V for 30 minutes. Following separation, gels were visualized and documented using a ChemiDoc™ Touch Imaging System (Bio-Rad).

2.7.6 HiFi DNA Assembly(Gibson Assembly) and Transformation

The reaction mixture is prepared according to the specified table and kept on ice. The mixture is then incubated in a thermocycler at 50°C for 15 minutes. After incubation, the samples are either stored on ice for immediate use or at -20°C for later transformation. For the transformation step, 2.0 µl (10%) of the chilled assembled product is used to transform NEB® 5-alpha Competent *E. coli* cells. These competent cells are either prepared in lab or can be purchased from NEB.

Parameter	**Amount**
DNA Molar Ratio	Vector:Insert = 1:2
Amount of Fragments	0.03 – 0.2 pmols
NEBuilder HiFi Assembly Master Mix	10 µl
Deionized H_2O	Up to 20 µl
Total Volume	20 µl

Thaw competent cells on ice. Around 5 ng (2 µl) of the DNA mixture is chilled in a 1.5 ml microcentrifuge tube. To this, 50 µl of competent cells are added and gently mixed by pipetting or flicking the tube 4-5 times, without vortexing. The mixture is then incubated on ice for 30 minutes without disturbance. Following this, the cells are heat-shocked at 42°C for 30 seconds without mixing. Next, 950 µl of room temperature media is added to the tube. The tube is then incubated at 37°C for 60 minutes with vigorous shaking at 250

rpm or rotation. Prior to plating, selection plates are warmed to 37°C. Finally, 50-100 µl of the cell and ligation mixture is spread onto the pre-warmed selection plates, which are then incubated overnight at 37°C to allow for colony formation.

2.7.7 Colony PCR for verification assembly, Cloning and knockout verification:

Component	Amount
DreamTaq PCR Master Mix (2X)	25 µL
Forward primer	0.1-1.0 µM
Reverse primer	0.1-1.0 µM
Template DNA	10 pg - 1 µg
Water, nuclease-free	to 50 µL
Total volume	50 µL

Thermocycler conditions:

Step	Temp	Time	Number of Cycles
Initial Denaturation	95	1-3 min	1
Denaturation	95	30 s	25-40
Annealing	T_m - 5	30 s	
Extension*	72	1 min	
Final extension	72	5 – 15 min	1

*NEB T_m calculator was used temperature

2.7.8 Electroporation:

P. putida competent cell preparation begins by centrifuging 500-750 µL of overnight culture at maximum speed for 30 seconds. The pellet is washed twice with 1 mL of 300 mM sucrose solution, centrifuging between washes. The final pellet is resuspended in 200 µL of sucrose solution. For transformation, plasmid DNA (750-1000 ng for pGNW or 40-100 ng for other plasmids) is added to the competent cells. This mixture is transferred

to a pre-chilled electroporation cuvette, ensuring the liquid is at the bottom. The cuvette is dried externally before placing it in the GenePulser Xcell Electroporator. Electroporation is performed using preset conditions (2.5 kV, 200 ohm, 25 µF). Immediately after pulsing, 0.9 mL of LB medium is added to the cuvette, and the entire contents are transferred to a clean 1.5 mL Eppendorf tube. The culture is incubated at 30°C for 1 hour with shaking at 500 rpm. Post-incubation, cells are either plated directly or concentrated by centrifugation. For the latter, cells are pelleted, resuspended in 100 µL LB, and spread on appropriate selective media. Plates are incubated inverted at 30°C overnight until colonies appear.

2.7.9 Metabolomics:

Sample quenching and metabolome extraction were performed to analyze both intracellular (endometabolome) and extracellular (exometabolome) metabolites. For sample quenching, 3 mL of cultures grown under the required conditions were rapidly mixed with 9 mL of pre-cooled methanol at -80°C. The quenched samples were then centrifuged at 10,000g for 10 minutes at -10°C. The supernatant was discarded, and the cell pellet was stored at -80°C for further processing. In parallel, 1 mL of culture was used to measure the optical density (OD_{600}) for normalization purposes.

For endometabolome extraction, the volume of extraction fluid was calculated based on the OD_{600} measurement. The extraction fluid consisted of 50% (v/v) methanol (LC-MS grade) and 50% TE buffer (10 mM TRIZMA, 1 mM EDTA, pH 7.0), stored at -20°C. The frozen cell pellets from the quenching step were thawed on ice, and the calculated volume of extraction fluid was added, followed by an equal volume of cold chloroform (-20°C). The mixture was vortexed in short intervals while maintaining a cool temperature until the pellet dispersed. The samples were then incubated in a shaker at maximum speed at -20°C for 2 hours. After incubation, the samples were centrifuged at maximum speed for 10 minutes at -10°C in a fixed-angle rotor. The upper phase, containing the polar metabolites, was carefully removed using a needle and filtered through a 0.2 µm PTFE membrane. The filtered extracts were then stored in microcentrifuge tubes at -20°C for further analysis.

For exometabolome preparation, 1 mL of culture was filtered through a 0.2 µm filter, followed by an additional filtration step using a 0.2 µm RC filter. The filtered extracellular samples were then stored at -20°C for subsequent analysis.

2.7.10 Growth phenotype measurement in Bioreactor:

Bioreactor experiments were done using the DASGIP® Parallel Bioreactor System. Following autoclave sterilization of the bioreactor vessel and assembly of components (DO/pH probes, gas lines), dissolved oxygen (DO) probes were calibrated to 100% air saturation using filtered air sparging. M9 minimal medium, prepared with defined carbon sources, was sterilized and loaded into the bioreactor. Throughout the experiment, temperature was maintained at 30°C via the integrated Bioblock system, while pH was automatically regulated at 7 using 1M HCl and 1M NaOH. CO_2 concentration was maintained at 5% of the gas mixture. DO levels were stabilized using adjustable agitation speeds(60–180 rpm) and filtered air injection, with baseline oxygen set to 18%. Optical density (OD) was tracked in real-time using infrared absorbance measurements (reported in arbitrary units). Cultures were inoculated at an initial OD_{600} of 0.05, with process parameters dynamically controlled via DASware software, which adjusted gas mixture (air/N_2/O_2/CO_2) to maintain stability. Aseptic sampling ports allowed periodic collection of culture samples (every 30–120 minutes) for OD_{600} measurements and substrate analysis.

2.7.11 Plasmid Curing

Plasmid curing is used to eliminate plasmids from bacterial cells. The process involves creating non-selective conditions by inoculating a plasmid-containing bacterial strain in LB media without antibiotics. The culture is then passaged multiple times though LB media to promote plasmid loss. After several passages, the bacterial culture is plated on both LB agar and LB agar supplemented with the appropriate antibiotic. Colonies that grow on LB agar but fail to grow on the antibiotic-containing plate are potential plasmid-cured isolates. To confirm plasmid curing, colony PCR is performed using plasmid-specific verification primers. The absence of amplification indicates successful plasmid elimination from the bacterial strain. This method allows for the selection and verification of plasmid-free bacterial colonies.

2.7.12 Gene deletions in *P. putida*:

To delete a specific genomic region, upstream (TS1) and downstream (TS2) regions of 500 base pairs flanking the target region were amplified using Q5 polymerase. These amplified fragments were joined by overlap extension PCR, resulting in segments of 1.0 kb. The segments were purified, typically as EcoRI-BamHI fragments, and ligated into the corresponding sites of the pEMG plasmid. The ligated plasmids were transformed into *E. coli* DH5αλpir for screening of ligation. Candidate clones were confirmed by full plasmid sequencing(Martínez-García & de Lorenzo, 2011). The resulting pEMG::flanking region plasmids were introduced into *P. putida* KT2440 through electroporation.

Since pEMG-derived plasmids cannot replicate in *P. putida*, kanamycin-resistant colonies appeared only when the plasmid co-integrated into the genome via homologous recombination. To resolve these co-integrates, the pSW-I plasmid was introduced either by electroporation. Transformants were selected on LB plates containing 500 µg/mL ampicillin(Martínez-García & de Lorenzo, 2011).

To induce resolution of co-integrates, stationary-phase cultures of the target strains were washed and diluted to an OD_{600} of 0.05 in LB medium containing ampicillin to maintain pSW-I. The cultures were treated with 15 mM 3-methyl benzoate and incubated further for up to six hours. Serial dilutions were plated on LB-Ap and LB-Ap/Km plates to determine the percentage of kanamycin-sensitive colonies, which indicated successful resolution of co-integrates toward either the wild-type genome or deletion mutants. PCRs with external primers were used to confirm deletions.

3. Results

3.1 Modular implementation of the CETCH cycle:

To streamline the implementation of the CETCH pathway, we divided it into four functional modules, allowing for stepwise integration and sequential monitoring of flux through the pathway. Building on previous work in *Escherichia coli* in the lab (Sánchez-Pascuala *et al*. *in preparation*), two plasmids expressing the required genes for converting crotonyl-CoA to succinyl-CoA within synthetic operons were designed and cloned, as illustrated in Fig. 6B. These operons were integrated into plasmids developed according to the SEVA (Standard European Vector Architecture) (Fig. 6A), which simplifies the exchange of genetic elements, enhances interoperability across microbial systems, and boosts the efficiency of genetic engineering (Martínez-García et al., 2023). Additionally, crotonyl-CoA ligase from *Pseudomonas aeruginosa* PAO1 (PA4198) was cloned into the plasmid to utilize external crotonate available in the media, since the cycle is not complete.

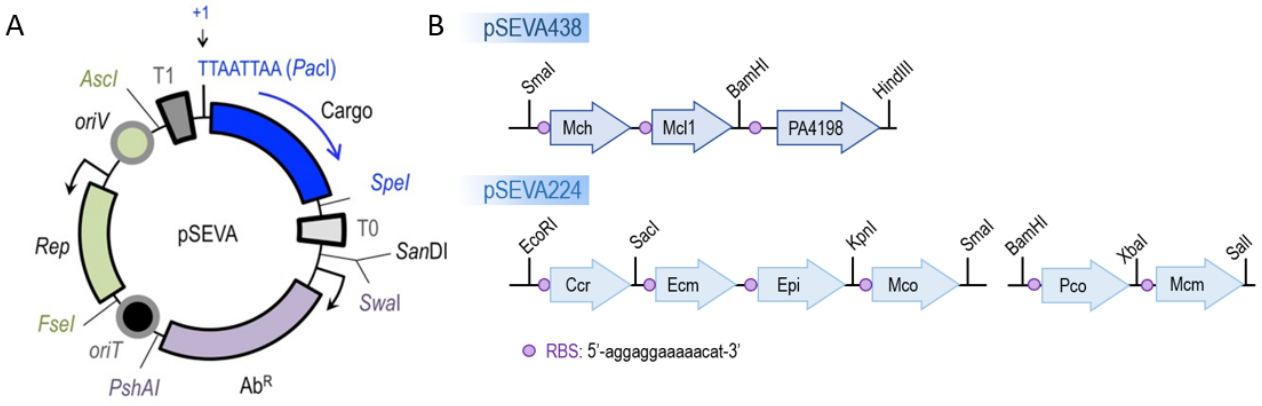

Figure 6 A) SEVA standard for plasmid design B) Synthetic operons used as cargo for expressing the CETCH cycle. Adapted from Sánchez-Pascuala et al. in preparation. PA198: *Pseudomonas aeruginosa* crotonyl CoA ligase; *oriV*: replication origin; *oriT*: replication origin for conjugation; T0, T1: terminator

sequences; RBS: Ribosome Binding Site; AsCI, PacI, SpeI, SanDI, SwaI, PshAI, FseI, SmaI, BamHI, HindIII, EcoRI, SacI, KpnI, SmaI, XbaI, SalI: Restriction Sites.

3.2 Methylmalonyl-CoA mutase (Mcm) and propionyl-CoA oxidase (Pco) activities are necessary to maximize the growth of *P. putida* KT2440 on crotonate *via* CETCH:

We initially aimed to characterize the growth phenotype of our strains in glucose with the supplementation of crotonate. To do this, we cultured both the empty vector (as a negative control) and CETCH-expressing strains CETCH(1)(2)(-mcm), metabolic profile as indicated in Fig. 7A, in minimal media supplemented with 20 mM glucose and in inducing conditions(Fig. 7C). Under these conditions, both the *P. putida* KT2440 transformed with empty plasmids [CETCH(-)] and the strain transformed with set of plasmids carrying the CETCH operon without the *mcm* gene [CETCH(1)(2)(-mcm)](Fig. 7B) strains achieved similar final optical densities (Fig. 7D). The slightly prolonged lag phase observed in the CETCH-expressing strain can be attributed to the increased protein burden from expressing multiple enzymes.

Next, we evaluated growth in the presence of glucose and 10 mM crotonate, where we observed a significant reduction in the growth of the CETCH(1)(2)(-mcm) strain (Fig. 7E).

We realized that this growth defect maybe due to *P. putida KT2440* lacking a native methylmalonyl-CoA mutase, as indicated by different databases (*i.e.* BioCyc, MaGe and The Pseudomonas Genome Database). Based on this we hypothesized that this growth reduction could be due to the accumulation of either acryloyl-CoA or propionyl-CoA in the CETCH(1)(2)(-mcm) strain, as metabolic flux cannot be redirected to Succinyl-CoA for biomass production or energy generation(Fig. 7A). Notably, both these metabolites are known to be toxic when accumulated within cells(Brock, 2010; Cao et al., 2017). To test this hypothesis, the methylmalonyl-CoA mutase (Mcm) was cloned into the operon (Fig. 7B) and growth was measured in media containing crotonate. This modification successfully alleviated the growth suppression associated with expressing the CETCH genes without Mcm activity in the presence of crotonate (Fig. 7E).

To further investigate the potential toxicity of metabolite accumulation, we conducted growth experiments using propionate as a substrate. In this condition, a native propionyl-CoA ligase would activate propionate, which could then either feed into the remaining segment of the CETCH cycle towards succinate or enter native propionate metabolism pathways through the methylcitrate pathway(Fig. S1A). This approach was expected to result in higher metabolite concentrations in these regions compared to growth on crotonate.

As anticipated, the CETCH(-) strain grew faster than the CETCH(1)(2)(+mcm) strain when cultured with propionate (Fig. S1b). This reduced growth in the CETCH(1)(2)(+mcm) strain suggests that a metabolite near propionate within the hortened CETCH pathway may be toxic. Furthermore, the CETCH(1)(2)(-mcm) strain failed to grow at all, potentially due to the accumulation of this toxic intermediate(Fig. S1B).

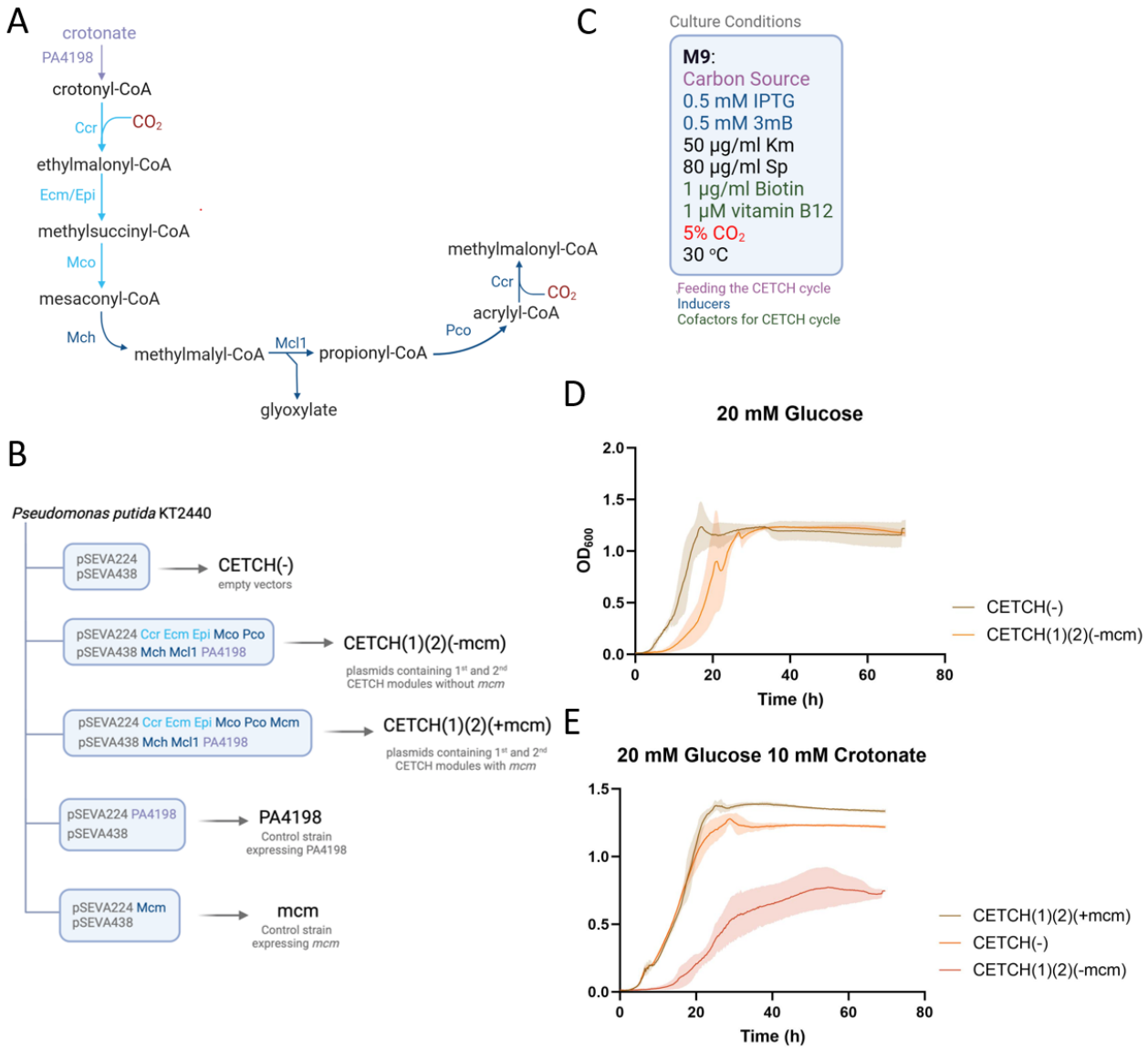

Figure 7 A) Schematic pathway in CETCH(1)(2)(-mcm) B) Strain notations and the representative genotypes C) Inducing conditions for CETCH expression D) Growth of CETCH(-) and CETCH(1)(2)(-mcm) in M9 20 mM glucose minimal medium. Shaded area represents standard deviation over three biological replicates. E) Growth of CETCH(-), CETCH(1)(2)(-mcm) and CETCH(1)(2)(+mcm) in M9 20 mM Glucose 10 mM crotonate. Shaded area represents standard deviation over three biological replicates.

3.3 Crotonate metabolism in *P. putida* KT2440 in combination with CETCH activities implementation:

The lack of growth defects in the strain encoding the CETCH activities (Fig. 7E) when using glucose and crotonate suggested that it may be possible to grow these cells in minimal media with only crotonate as a carbon source. This would significantly simplify future carbon labeling experiments by ensuring that metabolism occurs solely through a single carbon source. We first evaluated the growth in minimal media with 10 mM crotonate, where the CETCH (1)(2)(-mcm) strain exhibited no growth, while the CETCH(1)(2)(+mcm) strain grew substantially faster than the CETCH(-) strain (Fig. 8B). This supports our hypothesis regarding propionyl-CoA accumulation toxicity, as all crotonate in the -*mcm* strain is likely converted to propionyl-CoA under these conditions while once *mcm* is included it completes conversion into succinyl-CoA (Fig. 8A). To determine whether the observed recovery of growth was due to the combined effect of the CETCH activities and Mcm, rather than just the mutase alone, we expressed only the *mcm* gene (without the rest of the CETCH activities). This resulted in no improvement in growth (Fig. 8C). This further indicates that the partial CETCH pathway is functional in this context. Notably, we also observed that the CETCH(-) strain can grow on crotonate alone.

To investigate whether the rapid mobilization of crotonate *via P. aeruginosa* PAO1 crotonyl-CoA ligase (PA4198) accounts for the faster growth of the CETCH(1)(2)(+mcm) strain, we measured growth of a strain expressing only PA4198 in 20 mM crotonate. While the PA4198 strain demonstrated faster growth than the CETCH(-) strain, it did not grow as fast as the CETCH(1)(2)(+mcm) (Fig. 4c). The faster growth than CETCH(-) can be explained by the time taken for the native crotonyl-coA ligase to start getting expressed after adaptation to the new media or the native ligase being possibly less efficient than the one in *P. aeruginosa*. This suggests that while rapid mobilization of crotonate contributes to enhanced growth, nevertheless other genes within the CETCH pathway still play a significant role in the boosted crotonate metabolism.

To verify the observed growth phenotypes, we considered an alternative explanation for the slower growth of the empty vectors (EV) strain compared to the CETCH strain. We

hypothesized that the preculture conditions, specifically the use of glucose-containing media before measuring growth phenotypes, might influence the results. It was possible that the perceived growth benefit of the CETCH strain was due to the immediate overexpression of genes necessary for crotonate mobilisation, rather than the CETCH cycle itself. The EV strain might require time to adapt to crotonate-containing media by inducing and expressing the necessary genes for crotonate metabolism. To verify this hypothesis, we compared both strains using two different preculture conditions: one set precultured in glucose-containing media and another in crotonate-containing media. We then measured the growth phenotypes of these preconditioned strains. Interestingly, in both cases, the crotonate-preadapted strains exhibited growth patterns similar to those of the glucose-precultured strains (Fig. S1C). This observation provides further evidence that the improved growth phenotype is indeed attributable to the CETCH cycle rather than merely a difference in adaptation time to the crotonate-containing media.

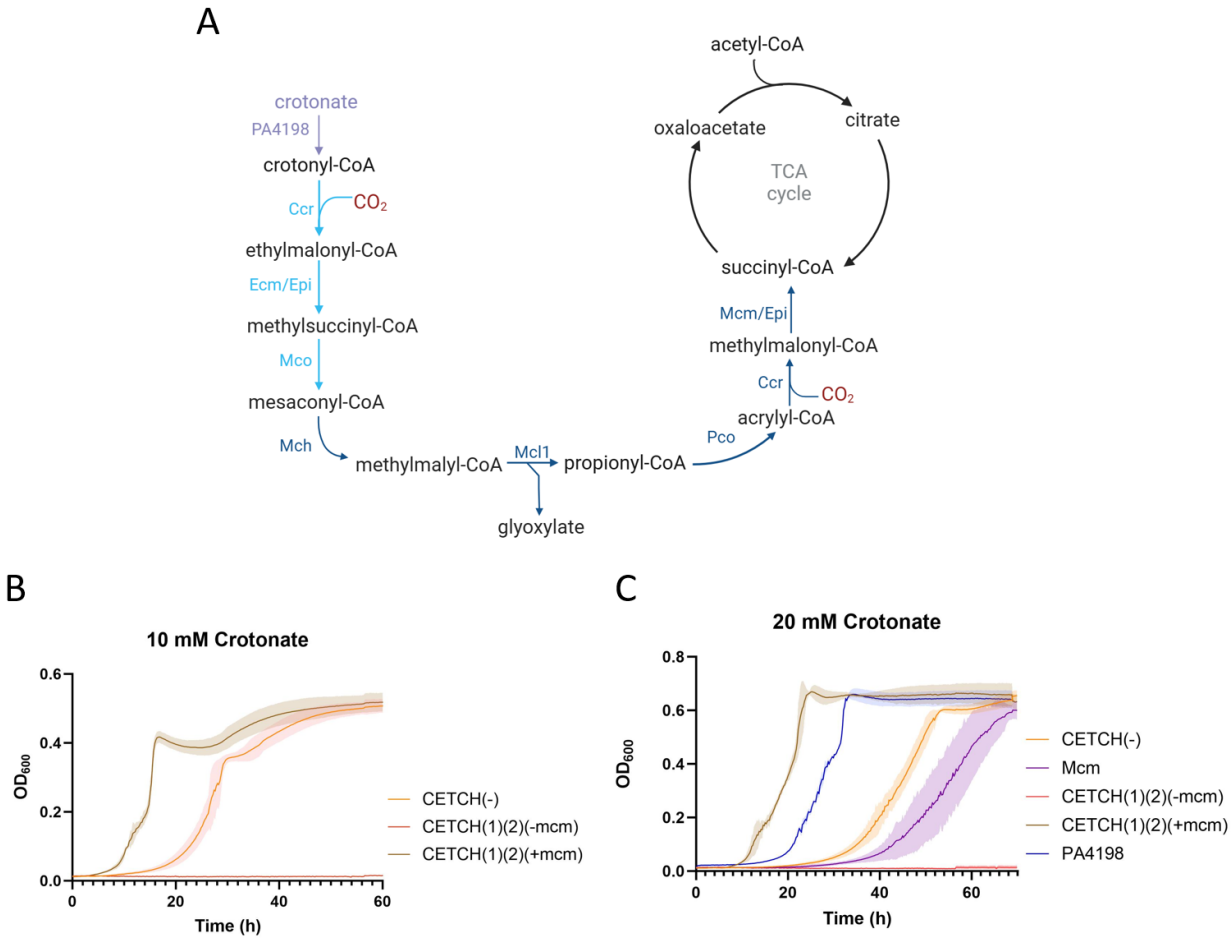

Figure 8 A) Schematic pathway in CETCH(1)(2)(+mcm) B) Growth of CETCH(-), CETCH(1)(2)(-mcm) and CETCH(1)(2)(+mcm) in 10 mM crotonate. Shaded area represents standard deviation over three biological replicates. C) Growth of CETCH(-), Mcm, PA4198 and CETCH(1)(2)(+mcm) in 20 mM crotonate ; growth experiments run in 5% CO_2. Shaded area represents standard deviation over three biological replicates.

3.4 CETCH(1)(2)(+mcm) shows diauxic growth in the bioreactor:

To assess the movement of CO_2 and crotonate within the central metabolism of *P. putida* KT2440, we planned to conduct metabolomics analyses. However, to accurately quantify these trace metabolites over time, a substantial biomass is required. Therefore, we opted to harvest cells using a bioreactor to maintain controlled culturing conditions and to achieve higher biomass yields.

We first characterized the growth of the CETCH(1)(2)(+mcm) and CETCH(-) strains in 20 mM crotonate medium within the bioreactor at 5% CO_2. As anticipated, the CETCH(1)(2)(+mcm) strain exhibited significantly faster growth (Figures 9A and 9B). Interestingly, this strain also demonstrated a diauxic growth pattern, as evidenced by both OD measurements and dissolved oxygen levels. Detailed analysis of dissolved oxygen (DO) dynamics showed us distinct metabolic patterns in both strains. The EV strain exhibited a mild diauxic growth pattern characterized by a 20-hour stagnation phase where oxygen consumption plateaued (DO stabilization lasting approximately 30 hours), indicating temporary metabolic arrest prior to resuming growth. This effect became amplified in the CETCH-expressing strain, which demonstrated two pronounced growth phases marked by oxygen depletion events. These phases showed direct correlation between optical density (OD) reductions and DO level fluctuations. We are currently uncertain which phase of exponential growth corresponds to the maximum activity of the CETCH pathway, necessitating the harvesting of samples from both phases for further analysis.

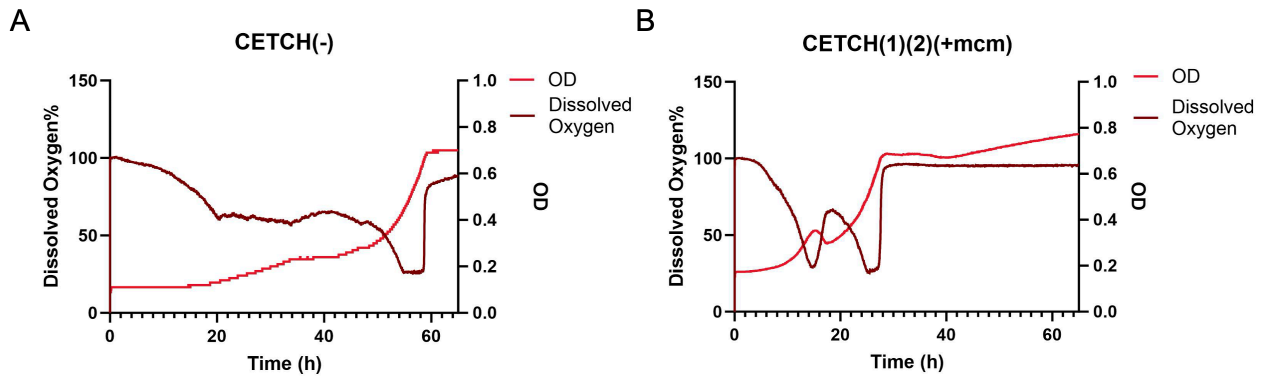

Figure 9 (A) Growth of CETCH(-) in a bioreactor. The brown line indicates the percentage of dissolved oxygen, normalized to 100% at the measurement taken before inoculation. The red line represents optical density (OD) measurements obtained via infrared, with the baseline set with 100% O_2 saturation with filtered air. (B) Diauxic growth of CETCH(1)(2)(+mcm) in a bioreactor. The brown line shows dissolved oxygen as a percentage, normalized to 100% at the pre-inoculation measurement. The red line depicts OD measurements using infrared, with the baseline calculated before inoculation.

3.5 Metabolomics shows limited flux within the CETCH cycle:

To assess metabolic flux through the CETCH cycle, we harvested *P. putida* cells at mid-exponential phase (OD_{600}~0.4) under inducing conditions and compared metabolite levels between strains expressing CETCH enzymes [CETCH(1)(2)(+mcm)] and an CETCH(-) control. The CETCH expressing strain exhibited significantly elevated crotonyl-CoA levels (Fig. 10A), consistent with the cycle's initial enzymatic activity. However, downstream metabolites (e.g., succinate, expected from TCA cycle entry of CETCH-derived succinyl-CoA) were either undetectable or showed no significant differences between strains (Fig. 10B and 10C), suggesting limited progression of intermediates through the full two modules of the CETCH. These results imply that while crotonyl-CoA production is robustly initiated in the CETCH strain, native side reactions likely divert intermediates away from the synthetic pathway, resulting in minimal net flux through the CETCH cycle. The data further suggest that crotonyl-CoA synthesis may represent the dominant metabolic route for crotonate assimilation in *P. putida*, with subsequent steps

in the CETCH cycle failing to outcompete endogenous metabolic processes for shared intermediates.

Our sampling, which provides a static snapshot of cellular metabolic activity, may have resulted in the failure to capture the optimal sampling time point for detecting metabolic flux through the CETCH pathway. Alternatively, the observed beneficial growth effects may stem from interactions between the engineered CETCH pathway and overlooked endogenous metabolic activities, rather than from the CETCH system functioning in isolation.

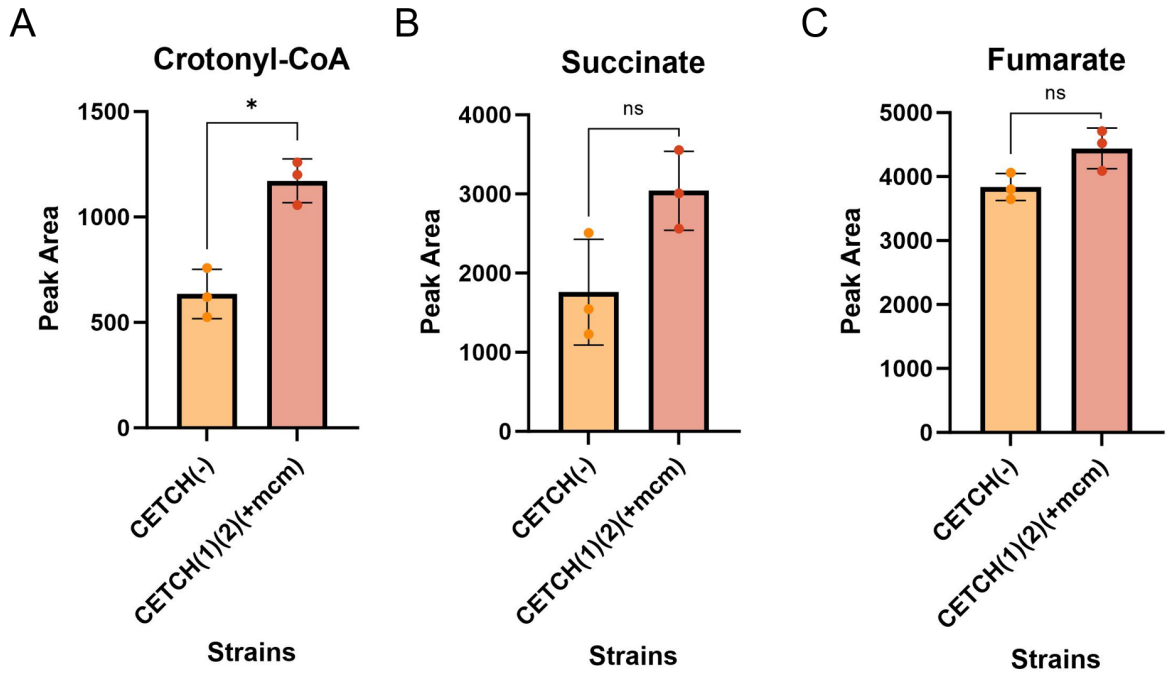

Figure 10 Quantification of key metabolites in CETCH(1)(2)(mcm) and CETCH(-) strains during mid-exponential growth on 10 mM crotonate. This analysis compares the metabolic profiles of the engineered CETCH(1)(2)(mcm) strain against the control CETCH(-) strain, focusing on the levels of A) crotonyl-CoA, B) succinate, and C) fumarate.

3.6 Crotonate metabolism in wild-type *P. putida* KT2440:

Since the CETCH(-) strain also exhibited growth on crotonate we were prompted to look into its entry points into central metabolism. Given that crotonyl-CoA is an intermediate in

the β-oxidation of even-numbered fatty acids larger than butyrate, we hypothesized that its utilization requires prior activation by a CoA ligase. Bioinformatic analyses using databases such as BioCyc revealed no annotated crotonyl-CoA ligases, which led us to consider that butyryl-CoA ligases may also possibly act as crotonyl-CoA ligase based on the substrate similarity.

Previous transposon mutagenesis data indicated PP_3553 (an annotated CoA ligase) showed significant fitness defects during growth on C4 fatty acids(Thompson et al., 2020). Amino acid sequence comparison showed high sequence similarity (83.15%) and modeling via AlphaFold showed high structural similarity (RMSD = 0.529) between PP_3553 and the characterized crotonyl-CoA ligase PA4198 from *P. aeruginosa* (Fig 11A)(Abramson et al., 2024). This prompted us to delete PP_3553. While the ΔPP_3553 mutant showed growth on glucose, it failed to grow in minimal media with crotonate as the sole carbon source (Fig 11B). Genetic complementation with PA4198 restored growth on crotonate as the sole carbon source, confirming PP_3553's role in crotonyl-CoA activation(Fig 11B).

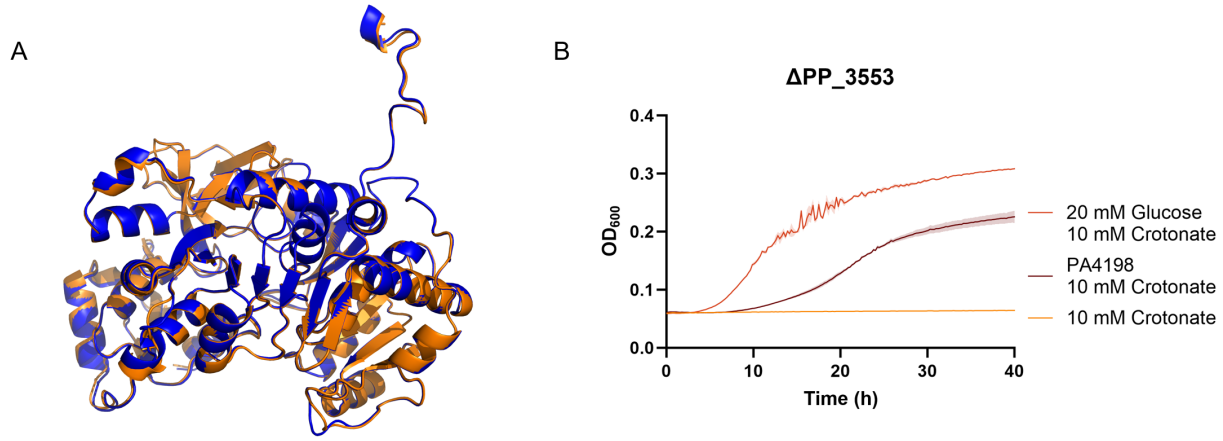

Figure 11 (A) Structural alignment of AlphaFold-predicted PP_3553 with PA4198, a characterized crotonyl-CoA ligase, highlighting conserved structural features. (B) Growth comparison of the *P. putida* KT2440 ΔPP_3553 strain under three conditions: 10 mM crotonate; 20 mM glucose supplemented with 10 mM crotonate; and 10 mM crotonate with heterologous overexpression of PA4198. Shaded area represents standard deviation over three biological replicates.

3.7 Engineering of P. putida to eliminate native crotonate metabolism:

To enhance flux through the CETCH cycle, we aimed to further restrict the pathway converting crotonate to acetyl-CoA, which is the primary route for crotonate to enter central metabolism. To achieve this we targeted a bottleneck reaction in the C4 β-oxidation pathway, specifically focusing on activities downstream of acyl-CoA dehydrogenase(Fig 12A). This strategy was chosen because most steps in the pathway are catalyzed by multiple genes, making complete elimination challenging. By selecting a reaction with the fewest gene-encoded activities, we could more effectively limit the conversion of crotonate to acetyl-CoA, potentially redirecting flux towards the CETCH cycle. This prompted us to knock out PP_2136(FadB), the primary enoyl-CoA hydratase, which shows moderate fitness defects with C4-length fatty acids and (Thompson et al., 2020). FadB can also act on the downstream at the level of the oxidation making it a promising candidate (Fig 12A).

Growth experiments showed that knocking out FadB caused reduction and not complete cessation of growth in crotonate possibly because of other redundant genes compensating to the β-oxidation functions(Fig 12B). Furthermore, the ΔFadB strain, when expressing the CETCH plasmids did not show any growth in crotonate (Fig 12E). We hypothesized that this maybe due to the unfavorable energy imbalance of the CETCH: producing one succinyl-CoA via CETCH requires two CO_2-fixation steps consuming 2 NADPH (equivalent to 5 ATP). The downstream conversion of succinyl-CoA to oxaloacetate generates only 1 ATP, 1 $FADH_2$, and 1 NADH (~5 ATP total), leaving no net energy surplus for cellular processes (Fig. 12C) given that all side-activities are removed. To mitigate this, we coupled CETCH with formate dehydrogenase-mediated NADPH regeneration, exploiting the strain's native genes (PP_2183-PP_2186) and supplementing 30 mM formate (Fig. 12D). This method gives the benefit of being able to provide energy without contributing to biomass. Under this condition we saw slight growth in the ΔFadB CETCH(1)(2)(+mcm) strain (Fig 12E). But this improvement cannot be attributed only to the CETCH given that even the ΔFadB CETCH(-) strain also exhibits improved growth rate (Fig 12 E).

A

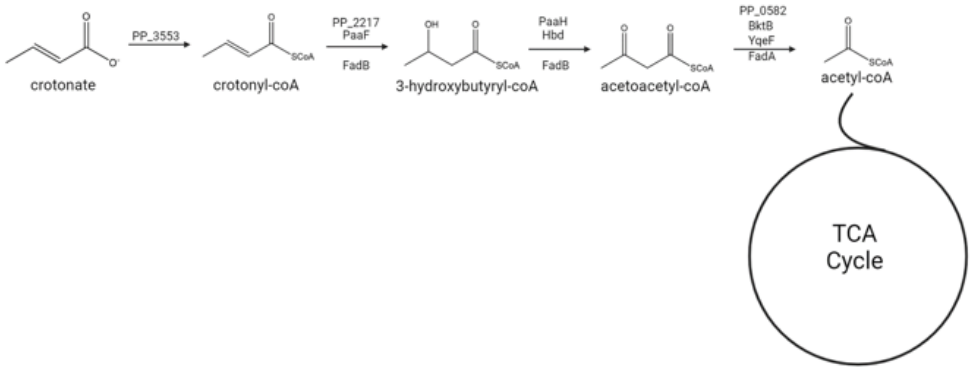
PP_3553
PP_2217
PaaF
FadB
PaaH
Hbd
FadB
PP_0582
BktB
YqeF
FadA
crotonate
crotonyl-coA
3-hydroxybutyryl-coA
acetoacetyl-coA
acetyl-coA
TCA
Cycle

B

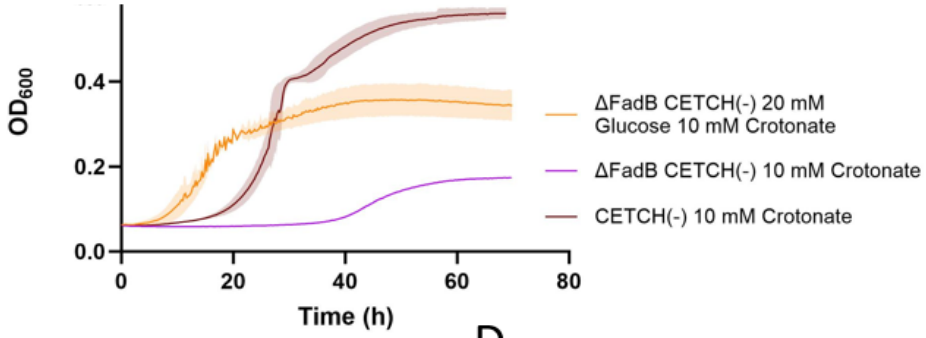
OD600
0.0
0.2
0.4
0
20
40
60
80
Time (h)
ΔFadB CETCH(-) 20 mM
Glucose 10 mM Crotonate
ΔFadB CETCH(-) 10 mM Crotonate
CETCH(-) 10 mM Crotonate

C

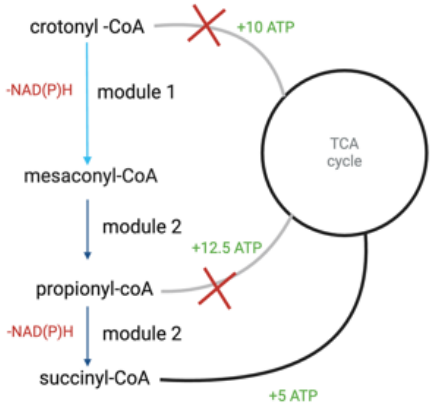
crotonyl -CoA
+10 ATP
-NAD(P)H
module 1
mesaconyl-CoA
module 2
+12.5 ATP
propionyl-coA
-NAD(P)H
module 2
succinyl-CoA
+5 ATP
TCA
cycle

D

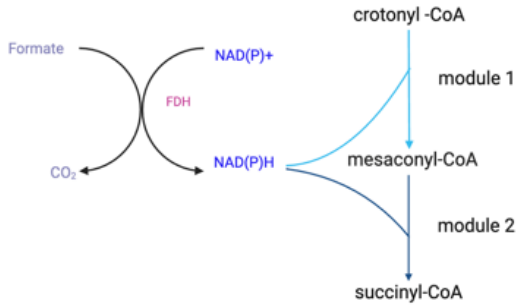
crotonyl -CoA
module 1
Formate
NAD(P)+
FDH
CO2
NAD(P)H
mesaconyl-CoA
module 2
succinyl-CoA

E

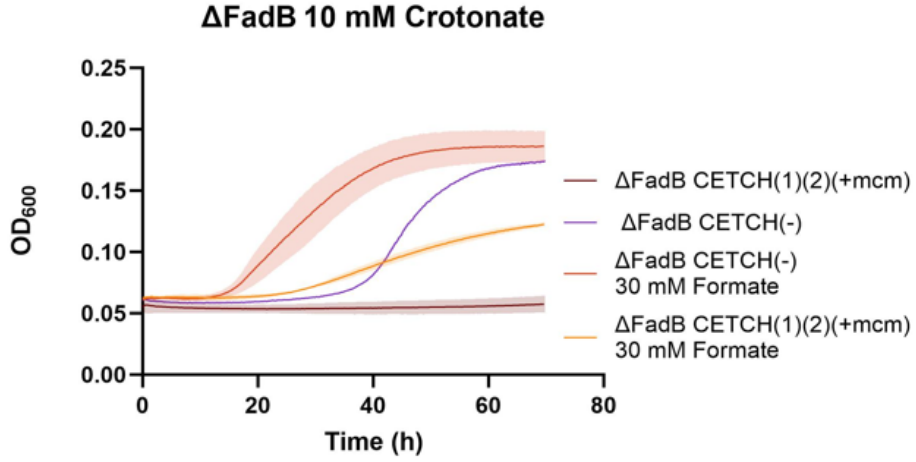
ΔFadB 10 mM Crotonate
OD600
0.00
0.05
0.10
0.15
0.20
0.25
0
20
40
60
80
Time (h)
ΔFadB CETCH(1)(2)(+mcm)
ΔFadB CETCH(-)
ΔFadB CETCH(-)
30 mM Formate
ΔFadB CETCH(1)(2)(+mcm)
30 mM Formate

Figure 12 A) Schematic representation of crotonate degradation via the β-oxidation pathway, yielding acetyl-CoA for entry into the tricarboxylic acid (TCA) cycle. (B) Growth comparison of the ΔFadB CETCH(-) strain under two conditions: 20 mM glucose; 10 mM crotonate and CETCH(-) supplemented with 10 mM crotonate. (C) Energy dynamics in the CETCH cycle: Production (green) from metabolic side reactions of cycle intermediates versus consumption (consumption) during key enzymatic steps. Side activities to be removed have been marked with a cross (red). (D) Schematic of a modular system for NADPH regeneration to power the CETCH cycle. Shaded area represents standard deviation over three biological replicates. (E) Growth comparison of ΔFadB strains with/without CETCH plasmids and with/without formate supplementation in 10 mM crotonate medium. Shaded area represents standard deviation over three biological replicates.

3.8 Further strain engineering for flux optimization:

To further optimize our strain for CETCH implementation, we created a double knockout of PP_3553 and FadB (Fig. 12B). This engineered strain behaved as hypothesized: it was unable to grow on crotonate alone, lacking the ability to convert crotonate to crotonyl-CoA, and showed no growth when harboring the CETCH plasmid due to insufficient energy production (Fig. 12B). However, the strain maintained robust growth on a mixture of 20 mM glucose and 10 mM crotonate.

We then attempted to increase CETCH cycle flux by targeting *prpC*, which encodes methyl citrate synthase, a key enzyme in the methyl citrate cycle that converts propionyl-CoA to pyruvate. Truncating this pathway would theoretically funnel more metabolites through the CETCH cycle (Fig. 12A). Despite successfully generating a cointegrate of our knockout plasmid with the *prpC* gene locus, we were unable to isolate any resolved strains with a confirmed *prpC* knockout, despite multiple attempts.

A

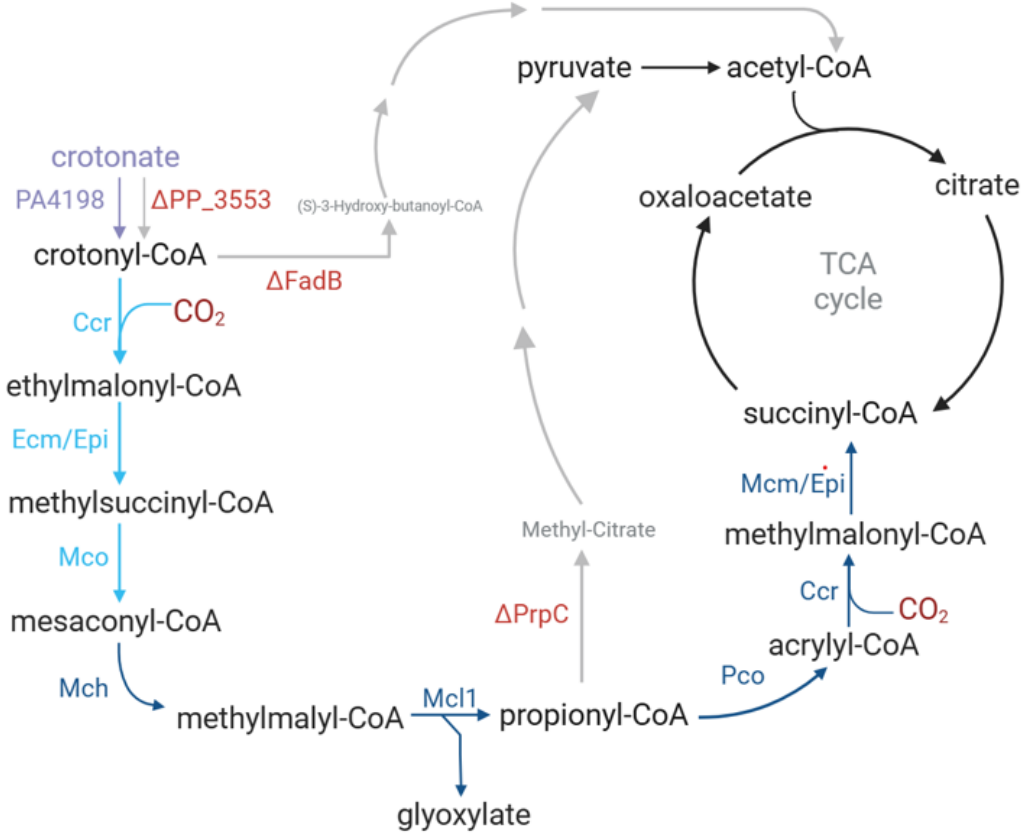
pyruvate
acetyl-CoA
crotonate
PA4198
ΔPP_3553
(S)-3-Hydroxy-butanoyl-CoA
oxaloacetate
citrate
crotonyl-CoA
ΔFadB
TCA
cycle
Ccr
CO2
ethylmalonyl-CoA
succinyl-CoA
Ecm/Epi
Mcm/Epi
methylsuccinyl-CoA
Methyl-Citrate
methylmalonyl-CoA
Mco
Ccr
CO2
ΔPrpC
mesaconyl-CoA
acrylyl-CoA
Pco
Mch
Mcl1
methylmalyl-CoA
propionyl-CoA
glyoxylate

B

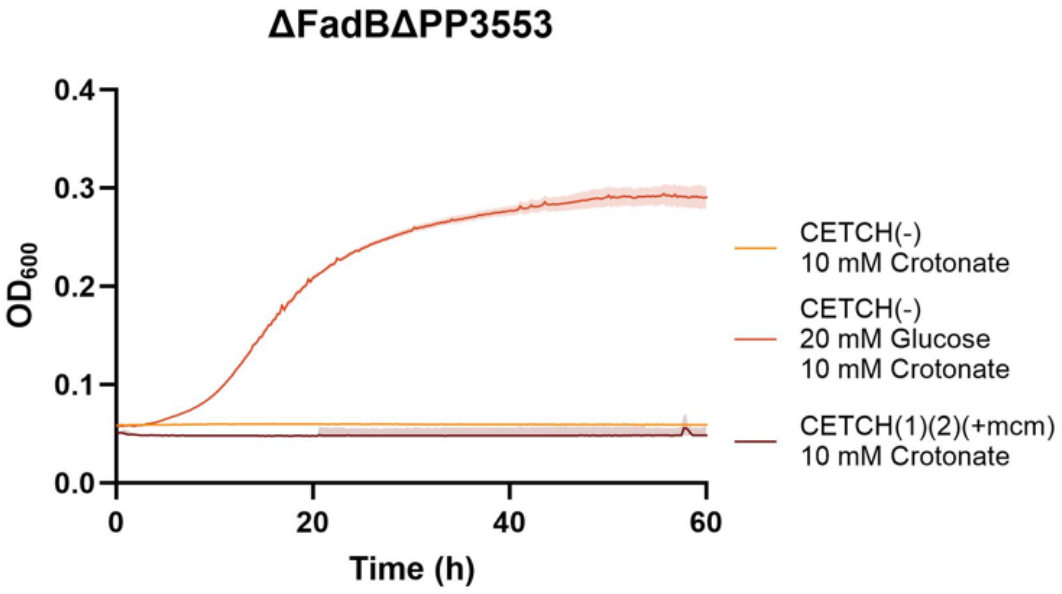
ΔFadBΔPP3553
OD600
0.4
0.3
0.2
0.1
0.0
0
20
40
60
Time (h)
CETCH(-)
10 mM Crotonate
CETCH(-)
20 mM Glucose
10 mM Crotonate
CETCH(1)(2)(+mcm)
10 mM Crotonate

Figure 13 A) Schematic illustrating the sequential gene deletions in P. putida designed to enhance metabolic flux through the CETCH cycle. B) Growth comparison of the ΔFadB ΔPP_3553 strain under different conditions: 10 mM crotonate and 20 mM glucose, 10 mM crotonate without the CETCH cycle, and 10 mM crotonate with the CETCH cycle. Shaded area represents standard deviation over three biological replicates.

3.9 Validation of CETCH activity through auxotrophic strains:

To further confirm CETCH activity in *P. putida*, we obtained two metabolic sensor strains for succinyl CoA and glyoxylate both key products within the CETCH from collaborators in the Systems Environmental Microbiology lab run by Dr. Pablo Nikel at the Center of Biosustainability at the Technical University of Denmark.

The engineered *P. putida strain* SEM11 Δ*sucABCD* Δ*aceA* Δ*scpC* Δ*aspC* serves as a metabolic sensor for succinyl-CoA levels through gene deletions that rewire cellular metabolism. The most important modification is the deletion of the *sucABCD* genes, which blocks the tricarboxylic acid (TCA) cycle. The *sucAB* (α-ketoglutarate dehydrogenase complex) deletion prevents the conversion of α-ketoglutarate to succinyl-CoA, while the *sucCD* (succinyl-CoA synthetase) deletion blocks the conversion of succinyl-CoA to succinate (Park et al., 1997). These deletions effectively disrupt the normal production and utilization of succinyl-CoA in the TCA cycle (Fig. 14A).

The *aceA* (isocitrate lyase) gene deletion disables the glyoxylate cycle, an alternative pathway that allows growth on two-carbon compounds like acetate (Díaz-Pérez et al., 2007). By removing this bypass, carbon flow is forced through pathways that might involve succinyl-CoA, further enhancing the sensor's sensitivity (Fig 14. A). The *scpC* gene deletion removes a CoA transferase involved in succinyl-CoA metabolism. This enzyme typically transfers the CoA moiety from succinyl-CoA to other organic acids (Haller et al., 2000). Its deletion limits alternative routes for succinyl-CoA production in the reverse direction. Finally, the *aspC* gene deletion restricts carbon flow between amino acid metabolism and the TCA cycle. *aspC* encodes aspartate aminotransferase (KURAMITSU et al., 1985), which connects these two metabolic pathways (Fig. 14A). Its removal potentially limits alternative routes that may produce succinyl-CoA levels,

through amino acids. Succinyl-CoA is an essential metabolite required for lysine biosynthesis. As a result, the strain's growth depends on the availability of succinyl-CoA, which can be supplied either through external supplementation of succinate or via an engineered metabolic pathway capable of producing succinyl-CoA. In the absence of either source, the strain will be unable to synthesize lysine and will not grow.

The second strain *P. putida* EM42 Δ*serA* Δ*itaE* Δ*aceA* serves as a metabolic sensor for glyoxylate. The *aceA* gene deletion blocks the primary route for glyoxylate production. The deletion of the *serA* gene removes 3-phosphoglycerate dehydrogenase activity (Zhang et al., 2017), thereby disrupting the canonical serine biosynthesis pathway that converts 3-phosphoglycerate to phosphoserine. This perturbation makes the organism auxotrophic for serine, as it can no longer synthesize this essential amino acid. To compensate, cellular serine pools must instead be generated via an alternative route: glycine serves as the sole precursor, which is itself synthesized through transamination of glyoxylate. In this auxotrophic strain, glyoxylate-derived glycine becomes critical for sustaining serine production, linking glyoxylate metabolism to amino acid homeostasis under these constrained metabolic conditions.

The results from these strains showed distinct sensor performance under different media conditions. In minimal media containing 10 mM glucose, both sensors differentiated between the presence and absence of succinate (Fig. 14B and Fig. S2A). However, when tested in a medium combining 10 mM glucose and 10 mM crotonate, only the succinyl-CoA sensor remained functional (Fig. 14C). While its signal intensity was reduced compared to glucose-only conditions, it still reliably distinguished between samples with and without succinate.

Given these findings, the succinyl-CoA sensor was selected for further use in the study. This decision was driven by its ability to operate effectively under dual-substrate conditions (glucose and crotonate), which mirror the metabolic environment of the CETCH cycle.

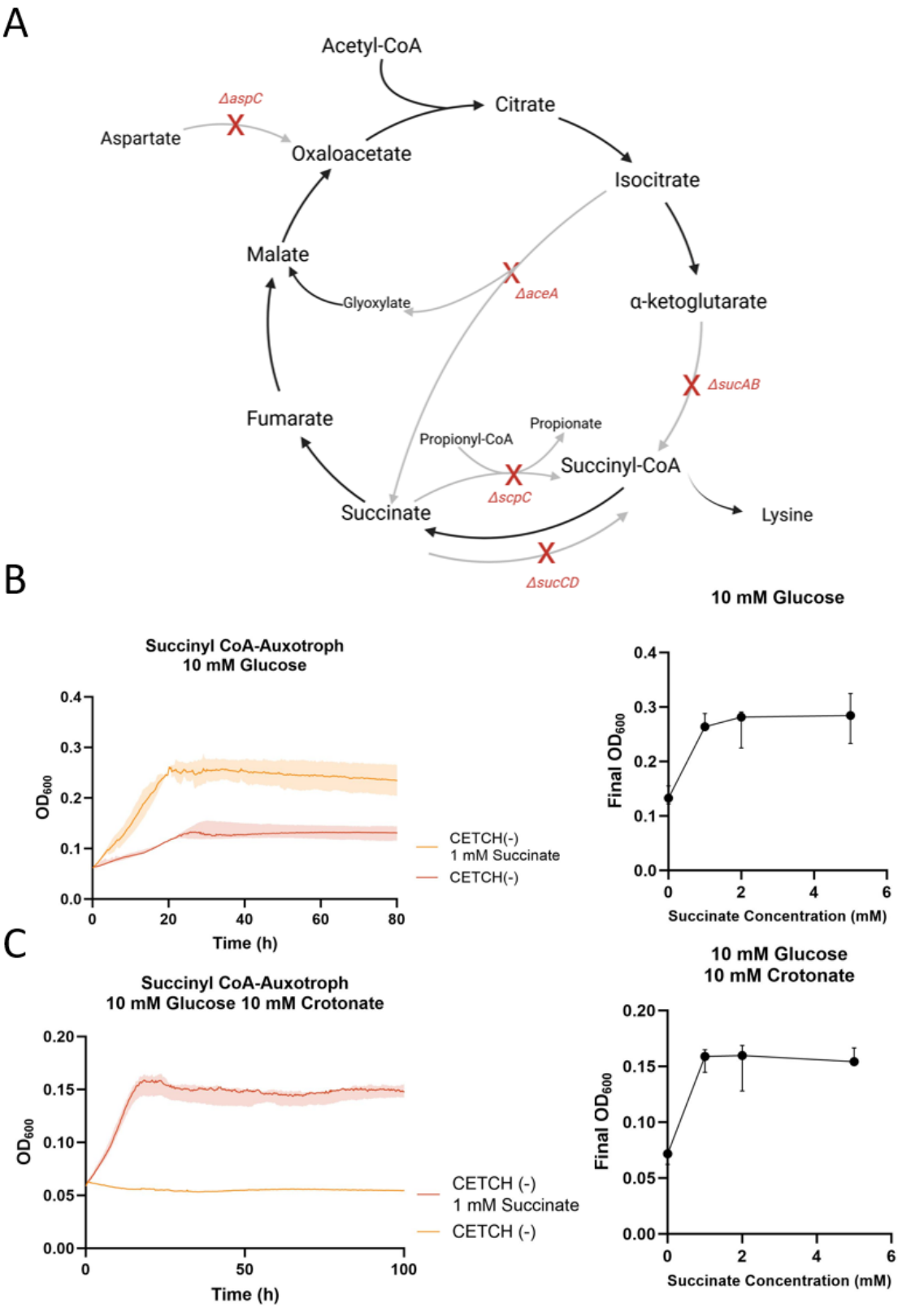
A
Acetyl-CoA
Citrate
Isocitrate
α-ketoglutarate
Succinyl-CoA
Succinate
Fumarate
Malate
Oxaloacetate
Aspartate
ΔaspC
Glyoxylate
ΔaceA
ΔsucAB
Propionyl-CoA
Propionate
ΔscpC
Lysine
ΔsucCD
B
10 mM Glucose
Succinyl CoA-Auxotroph
10 mM Glucose
OD600
Time (h)
CETCH(-)
1 mM Succinate
CETCH(-)
Final OD600
Succinate Concentration (mM)
C
10 mM Glucose
10 mM Crotonate
Succinyl CoA-Auxotroph
10 mM Glucose 10 mM Crotonate
OD600
Time (h)
CETCH (-)
1 mM Succinate
CETCH (-)
Final OD600
Succinate Concentration (mM)

Figure 14. A) Schematic depicting the gene deletions necessary to create a succinyl-CoA auxotroph. B) Growth comparison of the succinyl-CoA auxotroph in the presence and absence of succinate, as well as at different succinate concentrations, with 10 mM glucose as the carbon source. Shaded area represents standard deviation over three biological replicates. C) Growth comparison of the succinyl-CoA auxotroph in the presence and absence of succinate, and at varying succinate concentrations, with 10 mM glucose and 10 mM crotonate as carbon sources. Shaded area represents standard deviation over three biological replicates.

3.10 Validation of CETCH activity through the Succinyl-CoA Auxotroph

Following the successful characterization of a Succinyl-CoA sensor suitable for our experimental conditions, we introduced the CETCH plasmids into the sensor strain. Surprisingly, no growth was observed in glucose and crotonate media, even when supplemented with succinate at concentrations that supported growth in strains carrying empty vector plasmids (Fig. 15B). We hypothesized that this growth inhibition might be attributed to an increased succinyl-CoA demand imposed by the CETCH cycle. To address this decided to either increase succinate supply in the medium or reduce intracellular succinyl-CoA demand. We opted for the latter approach by targeting the trans-sulfurylation pathway involved in methionine biosynthesis. This pathway utilizes the MetA enzyme, which specifically requires succinyl-CoA to produce O-succinylhomoserine, a precursor in methionine synthesis (Alaminos & Ramos, 2001). By supplementing the media with methionine, we aimed to partially alleviate the succinyl-CoA demand from this pathway (Fig. 15A).

Methionine supplementation was able to successfully restore growth of the CETCH-containing strain to levels comparable with the empty vector control when cultured in the presence of succinate (Fig 15. C). However, growth remained inhibited in the absence of exogenous succinate. To further optimize growth conditions, we introduced formate to the media, hypothesizing that it could generate additional reducing power to potentially overcome CETCH-related metabolic constraints. This approach, utilizing both methionine and formate supplementation, resulted in a consistent, albeit limited, growth phenotype characterized by a single doubling in the absence of succinate (Fig. 15C).

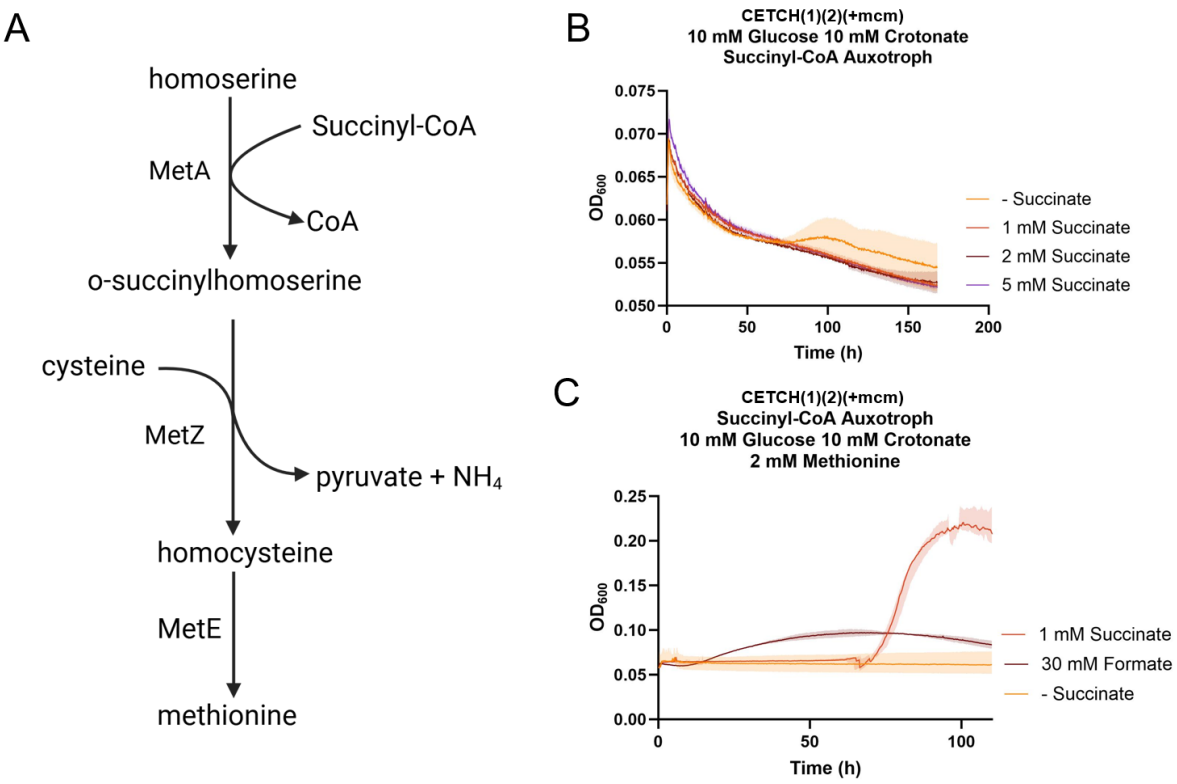

Figure 15. (A) Schematic illustration of the trans-sulfurylation pathway in *P. putida*. (B) Growth performance of the succinyl-CoA auxotrophic strain engineered with the CETCH pathway in minimal media supplemented with 10 mM glucose and 10 mM crotonate. (C) Growth evaluation of the same strain under identical media conditions with additional supplementation of 2 mM methionine and varying metabolites: no succinate(- succinate), 1 mM succinate, or 30 mM formate.

3.10 Evolution of Succinyl-CoA Auxotroph with CETCH activity towards improved growth:

After successfully achieving a single doubling in the CETCH-expressing succinyl-CoA sensor strain, we aimed to evolve this strain to achieve a higher final OD_{600}. The strain was cultured under selective conditions until it reached its maximum OD_{600}, followed by dilution into fresh media under inducing conditions supplemented with 1 mM succinate in a 5% CO_2 atmosphere. After six cycles of such serial passages, we obtained a strain capable of reaching a maximum OD_{600} of 1. This evolved strain also demonstrated

resistance to kanamycin and spectinomycin and no longer required formate, methionine, or succinate for growth when cultured in 10 mM glucose and 10 mM crotonate.

4. Discussion and Outlook

Our research has demonstrated improved growth of the CETCH(1)(2)(+mcm) strain, which is surprising despite multiple controls. This suggests that the CETCH cycle provides a fitness advantage during growth on crotonate, although it's possible that only a subset of CETCH activities is responsible for this advantage. One possible way to parse this is to combinatorially express the CETCH genes to find out the combination that maximally provides advantage.

We identified a potential native pathway for crotonate metabolism in wild-type *P. putida* KT-2440, likely through fatty acid synthetic-degradation pathways. To investigate crotonate entry into native metabolism, we knocked out the putative enoyl-CoA ligase PP_3553, active on C4 compounds. The knockout strain's growth phenotype revealed a new activity of PP_3553 in crotonate metabolism, likely through CoA activation. This claim is supported by the protein's structural similarity to other CoA-ligases and the ability of PA4198, a known crotonyl-CoA ligase, to recover growth. The PP_3553 knockout strain we developed presents significant potential for future research and biotechnological applications. One particularly promising avenue is its use in crotonate production. Previous attempts to produce crotonate have been hampered by the tendency of cells to consume the produced crotonate, limiting overall yield. Our knockout strain, with its impaired ability to metabolize crotonate, could overcome this limitation. By reducing or eliminating the cell's capacity to catabolize crotonate, this strain could serve as an excellent platform for engineered crotonate production pathways, potentially leading to higher yields and more efficient production processes. This characteristic makes our knockout strain a valuable tool for metabolic engineering efforts aimed at crotonate biosynthesis and other related compounds.

While we significantly were able to reduce growth on crotonate-only media using a FadB knockout, complete growth restriction was not achieved. The redundant gene PP_2217,

which can also act as an enoyl-CoA hydratase, may be a candidate for knockout to fully restrict crotonate growth, given that a transposon insertion into this gene restricts growth in butyrate(Thompson et al., 2020). We hypothesize that crotonate may enter native central metabolism via the methyl citrate cycle after partial processing through CETCH modules, converting propionyl-CoA into pyruvate and feeding directly into the TCA cycle. Attempts to knockout *prpC* (methyl citrate synthase) have been unsuccessful, possibly due to its essential nature in this background. The challenge of balancing crotonate utilization for energy and maintaining the CETCH pathway could potentially be addressed by adding glucose for energy production or introducing a simpler substrate that provides energy and reducing power without contributing to carbon metabolism. This approach could enable future adaptive laboratory evolution experiments.

Our experimental validation of glyoxylate and succinyl-CoA biosensors revealed distinct growth dependencies in the engineered strain. The succinyl-CoA-dependent sensor strain exhibited conditional growth, achieving measurable biomass accumulation only when partially supplemented with formate and methionine. This suggests suboptimal metabolic flux through the engineered pathway, potentially due to kinetic bottlenecks in cofactor recycling or insufficient enzyme activity.

Through directed evolution, we obtained an optimized sensor strain harboring the CETCH plasmid, which demonstrated significantly enhanced growth on succinate as the sole carbon source, achieving a four-fold increase in maximum OD_{600} compared to the parental strain. While this phenotypic improvement indicates adaptive optimization, the mechanistic basis remains unresolved. Two non-exclusive hypotheses can be possible in this context: compensatory mutations in pathways supporting CETCH function, or the emergence of latent enzymatic activities enabling auxiliary carbon assimilation. Verifying these hypotheses will require plasmid curing to assess trait heritability, comparative ^{13}C metabolic flux analysis between strains, and proteomic profiling of redox-cofactor balancing systems.

The sensor's design inherently creates weak evolutionary selection pressure due to its reliance on succinyl-CoA's role as a lysine and cell wall biosynthesis cofactor rather than a carbon source. This low-stringency selection likely permits the accumulation of bypass

mutations through multiple mechanisms. Thus evolution may have biased towards this outcome when compared to the improvements in CETCH. Additionally, regulatory network rewiring under prolonged selection could derepress silent metabolic genes. Notably, while *P. putida* and *E. coli* utilize N-succinyl-L,L-diaminopimelic acid as their lysine precursor, *Bacillus subtilis* employs an evolutionarily distinct acetyl-CoA-dependent pathway along with the succinyl-CoA pathway(*KEGG PATHWAY: Lysine Biosynthesis - Bacillus subtilis BSn5*, n.d.). The evolved strain's phenotype could theoretically through a similar convergent evolution of the pathway architecture.

Our study demonstrates partial CETCH pathway implementation in *P. putida* KT2440 and evolution of a promising candidate strain with improved growth characteristics. To resolve the mechanistic reasons of these improvements, combining whole-genome sequencing of evolved lineages, comparative transcriptomics under varying carbon sources (succinate/glucose/crotonate) along with carbon labelling experiments would be needed. These would distinguish between adaptive mutations enhancing CETCH efficiency and selection-escaping adaptations, providing insights for engineering evolutionarily stable synthetic metabolic networks.

5. References

Abramson, J., Adler, J., Dunger, J., Evans, R., Green, T., Pritzel, A., Ronneberger, O., Willmore, L., Ballard, A. J., Bambrick, J., Bodenstein, S. W., Evans, D. A., Hung, C.-C., O'Neill, M., Reiman, D., Tunyasuvunakool, K., Wu, Z., Žemgulytė, A., Arvaniti, E., … Jumper, J. M. (2024). Accurate structure prediction of biomolecular interactions with AlphaFold 3. *Nature*, *630*(8016), 493–500. https://doi.org/10.1038/s41586-024-07487-w

Alaminos, M., & Ramos, J. L. (2001). The methionine biosynthetic pathway from homoserine in Pseudomonas putida involves the metW, metX, metZ, metH and metE gene products. *Archives of Microbiology*, *176*(1), 151–154. https://doi.org/10.1007/s002030100293

AR6 Synthesis Report: Climate Change 2023. (n.d.). Retrieved October 14, 2024, from https://www.ipcc.ch/report/ar6/syr/

Bar-Even, A., Noor, E., Lewis, N. E., & Milo, R. (2010). Design and analysis of synthetic carbon fixation pathways. *Proceedings of the National Academy of Sciences*, *107*(19), 8889–8894. https://doi.org/10.1073/pnas.0907176107

Bernhardsgrütter, I., Schell, K., Peter, D. M., Borjian, F., Saez, D. A., Vöhringer-Martinez, E., & Erb, T. J. (2019). Awakening the Sleeping Carboxylase Function of Enzymes: Engineering the Natural CO2-Binding Potential of Reductases. *Journal of the American Chemical Society*, *141*(25), 9778–9782. https://doi.org/10.1021/jacs.9b03431

Brock, M. (2010). Role of Cellular Control of Propionyl-CoA Levels for Microbial Pathogenesis. In K. N. Timmis (Ed.), *Handbook of Hydrocarbon and Lipid*

Microbiology (pp. 3279–3291). Springer. https://doi.org/10.1007/978-3-540-77587-4_249

Cao, H.-Y., Wang, P., Xu, F., Li, P.-Y., Xie, B.-B., Qin, Q.-L., Zhang, Y.-Z., Li, C.-Y., & Chen, X.-L. (2017). Molecular Insight into the Acryloyl-CoA Hydration by AcuH for Acrylate Detoxification in Dimethylsulfoniopropionate-Catabolizing Bacteria. *Frontiers in Microbiology*, *8*. https://doi.org/10.3389/fmicb.2017.02034

Chavarría, M., Nikel, P. I., Pérez-Pantoja, D., & de Lorenzo, V. (2013). The Entner–Doudoroff pathway empowers seudomonas putida KT2440 with a high tolerance to oxidative stress. *Environmental Microbiology*, *15*(6), 1772–1785. https://doi.org/10.1111/1462-2920.12069

Claassens, N. J., Scarinci, G., Fischer, A., Flamholz, A. I., Newell, W., Frielingsdorf, S., Lenz, O., & Bar-Even, A. (2020). Phosphoglycolate salvage in a chemolithoautotroph using the Calvin cycle. *Proceedings of the National Academy of Sciences*, *117*(36), 22452–22461. https://doi.org/10.1073/pnas.2012288117

Climate Change: Atmospheric Carbon Dioxide | NOAA Climate.gov. (2024, April 9). https://www.climate.gov/news-features/understanding-climate/climate-change-atmospheric-carbon-dioxide

Cotton, C. A., Edlich-Muth, C., & Bar-Even, A. (2018). Reinforcing carbon fixation: CO2 reduction replacing and supporting carboxylation. *Current Opinion in Biotechnology*, *49*, 49–56. https://doi.org/10.1016/j.copbio.2017.07.014

de Lorenzo, V., Pérez-Pantoja, D., & Nikel, P. I. (2024). Pseudomonas putida KT2440: The long journey of a soil-dweller to become a synthetic biology chassis. *Journal of Bacteriology*, *206*(7), e00136-24. https://doi.org/10.1128/jb.00136-24

Díaz-Pérez, A. L., Román-Doval, C., Díaz-Pérez, C., Cervantes, C., Sosa-Aguirre, C. R., López-Meza, J. E., & Campos-García, J. (2007). Identification of the aceA gene encoding isocitrate lyase required for the growth of Pseudomonas aeruginosa on acetate, acyclic terpenes and leucine. *FEMS Microbiology Letters*, *269*(2), 309–316. https://doi.org/10.1111/j.1574-6968.2007.00654.x

Eltbaakh, Y. A., Ruslan, M. H., Alghoul, M. A., Othman, M. Y., Sopian, K., & Razykov, T. M. (2012). Solar attenuation by aerosols: An overview. *Renewable and Sustainable Energy Reviews*, *16*(6), 4264–4276. https://doi.org/10.1016/j.rser.2012.03.053

Emissions from Fossil Fuels Continue to Rise. (2024, March 5). [Text.Article]. NASA Earth Observatory. https://earthobservatory.nasa.gov/images/152519/emissions-from-fossil-fuels-continue-to-rise

Erb, T. J. (2024). Photosynthesis 2.0: Realizing New-to-Nature CO2-Fixation to Overcome the Limits of Natural Metabolism. *Cold Spring Harbor Perspectives in Biology*, *16*(2), a041669. https://doi.org/10.1101/cshperspect.a041669

Erb, T. J., Berg, I. A., Brecht, V., Müller, M., Fuchs, G., & Alber, B. E. (2007). Synthesis of C_5 -dicarboxylic acids from C_2 -units involving crotonyl-CoA carboxylase/reductase: The ethylmalonyl-CoA pathway. *Proceedings of the National Academy of Sciences*, *104*(25), 10631–10636. https://doi.org/10.1073/pnas.0702791104

Erb, T. J., Brecht, V., Fuchs, G., Müller, M., & Alber, B. E. (2009). Carboxylation mechanism and stereochemistry of crotonyl-CoA carboxylase/reductase, a carboxylating enoyl-thioester reductase. *Proceedings of the National Academy of Sciences*, *106*(22), 8871–8876. https://doi.org/10.1073/pnas.0903939106

Erb, T. J., & Zarzycki, J. (2018). A short history of RubisCO: The rise and fall (?) of Nature's predominant CO2 fixing enzyme. *Current Opinion in Biotechnology*, *49*, 100–107. https://doi.org/10.1016/j.copbio.2017.07.017

Flamholz, A., Noor, E., Bar-Even, A., Liebermeister, W., & Milo, R. (2013). Glycolytic strategy as a tradeoff between energy yield and protein cost. *Proceedings of the National Academy of Sciences*, *110*(24), 10039–10044. https://doi.org/10.1073/pnas.1215283110

Gross, F., Ring, M. W., Perlova, O., Fu, J., Schneider, S., Gerth, K., Kuhlmann, S., Stewart, A. F., Zhang, Y., & Müller, R. (2006). Metabolic Engineering of *Pseudomonas putida* for Methylmalonyl-CoA Biosynthesis to Enable Complex Heterologous Secondary Metabolite Formation. *Chemistry & Biology*, *13*(12), 1253–1264. https://doi.org/10.1016/j.chembiol.2006.09.014

H, E., E, T., V, O., E, P., & A, L. (2009). Rubisco in planta kcat is regulated in balance with photosynthetic electron transport. *Journal of Experimental Botany*, *60*(14). https://doi.org/10.1093/jxb/erp242

Haller, T., Buckel, T., Rétey, J., & Gerlt, J. A. (2000). Discovering New Enzymes and Metabolic Pathways: Conversion of Succinate to Propionate by Escherichia coli. *Biochemistry*, *39*(16), 4622–4629. https://doi.org/10.1021/bi992888d

Kaste, J. A., Walker, B. J., & Shachar-Hill, Y. (2024). Biophysical carbon concentrating mechanisms in land plants: Insights from reaction-diffusion modeling. *bioRxiv*, 2024.01.04.574220. https://doi.org/10.1101/2024.01.04.574220

KEGG PATHWAY: Lysine biosynthesis—Bacillus subtilis BSn5. (n.d.). Retrieved March 11, 2025, from https://www.genome.jp/kegg-bin/show_pathway?bsn00300

KURAMITSU, S., OKUNO, S., OGAWA, T., OGAWA, H., & KAGAMIYAMA, H. (1985). Aspartate Aminotransferase of Escherichia coli: Nucleotide Sequence of the aspC Gene1. *The Journal of Biochemistry*, *97*(4), 1259–1262. https://doi.org/10.1093/oxfordjournals.jbchem.a135173

Loder, A. J., Han, Y., Hawkins, A. B., Lian, H., Lipscomb, G. L., Schut, G. J., Keller, M. W., Adams, M. W. W., & Kelly, R. M. (2016). Reaction kinetic analysis of the 3-hydroxypropionate/4-hydroxybutyrate CO2 fixation cycle in extremely thermoacidophilic archaea. *Metabolic Engineering*, *38*, 446–463. https://doi.org/10.1016/j.ymben.2016.10.009

Löwe, H., & Kremling, A. (2021). In-Depth Computational Analysis of Natural and Artificial Carbon Fixation Pathways. *BioDesign Research*, *2021*, 9898316. https://doi.org/10.34133/2021/9898316

Lüthi, D., Le Floch, M., Bereiter, B., Blunier, T., Barnola, J.-M., Siegenthaler, U., Raynaud, D., Jouzel, J., Fischer, H., Kawamura, K., & Stocker, T. F. (2008). High-resolution carbon dioxide concentration record 650,000–800,000 years before present. *Nature*, *453*(7193), 379–382. https://doi.org/10.1038/nature06949

Manoli, M.-T., Nogales, J., & Prieto, A. (n.d.). Synthetic Control of Metabolic States in Pseudomonas putida by Tuning Polyhydroxyalkanoate Cycle. *mBio*, *13*(1), e01794-21. https://doi.org/10.1128/mbio.01794-21

Martínez-García, E., & de Lorenzo, V. (2011). Engineering multiple genomic deletions in Gram-negative bacteria: Analysis of the multi-resistant antibiotic profile of Pseudomonas putida KT2440. *Environmental Microbiology*, *13*(10), 2702–2716. https://doi.org/10.1111/j.1462-2920.2011.02538.x

Martínez-García, E., Fraile, S., Algar, E., Aparicio, T., Velázquez, E., Calles, B., Tas, H., Blázquez, B., Martín, B., Prieto, C., Sánchez-Sampedro, L., Nørholm, M. H. H., Volke, D. C., Wirth, N. T., Dvořák, P., Alejaldre, L., Grozinger, L., Crowther, M., Goñi-Moreno, A., … de Lorenzo, V. (2023). SEVA 4.0: An update of the Standard European Vector Architecture database for advanced analysis and programming of bacterial phenotypes. *Nucleic Acids Research*, *51*(D1), D1558–D1567. https://doi.org/10.1093/nar/gkac1059

Martínez-García, E., Nikel, P. I., Aparicio, T., & de Lorenzo, V. (2014). Pseudomonas 2.0: Genetic upgrading of P. putida KT2440 as an enhanced host for heterologous gene expression. *Microbial Cell Factories*, *13*(1), 159. https://doi.org/10.1186/s12934-014-0159-3

Nakazawa, T. (2003). Travels of a Pseudomonas, from Japan around the world. *Environmental Microbiology*, *5*(1), 78–78. https://doi.org/10.1046/j.1462-2920.2002.00269.x-i1

Nikel, P. I., Chavarría, M., Fuhrer, T., Sauer, U., & de Lorenzo, V. (2015). *Pseudomonas putida* KT2440 Strain Metabolizes Glucose through a Cycle

Formed by Enzymes of the Entner-Doudoroff, Embden-Meyerhof-Parnas, and Pentose Phosphate Pathways*. *Journal of Biological Chemistry*, *290*(43), 25920–25932. https://doi.org/10.1074/jbc.M115.687749

Orsi, E., Claassens, N. J., Nikel, P. I., & Lindner, S. N. (2021). Growth-coupled selection of synthetic modules to accelerate cell factory development. *Nature Communications*, *12*(1), 5295. https://doi.org/10.1038/s41467-021-25665-6

Park, S. J., Chao, G., & Gunsalus, R. P. (1997). Aerobic regulation of the sucABCD genes of Escherichia coli, which encode alpha-ketoglutarate dehydrogenase and succinyl coenzyme A synthetase: Roles of ArcA, Fnr, and the upstream sdhCDAB promoter. *Journal of Bacteriology*, *179*(13), 4138–4142. https://doi.org/10.1128/jb.179.13.4138-4142.1997

Sage, R. F. (2002). Variation in the kcat of Rubisco in C3 and C4 plants and some implications for photosynthetic performance at high and low temperature. *Journal of Experimental Botany*, *53*(369), 609–620. https://doi.org/10.1093/jexbot/53.369.609

Sánchez-Pascuala, A., Fernández-Cabezón, L., de Lorenzo, V., & Nikel, P. I. (2019). Functional implementation of a linear glycolysis for sugar catabolism in *Pseudomonas putida*. *Metabolic Engineering*, *54*, 200–211. https://doi.org/10.1016/j.ymben.2019.04.005

Santos Correa, S., Schultz, J., Lauersen, K. J., & Soares Rosado, A. (2023). Natural carbon fixation and advances in synthetic engineering for redesigning and creating new fixation pathways. *Journal of Advanced Research*, *47*, 75–92. https://doi.org/10.1016/j.jare.2022.07.011

Schulz-Mirbach, H., Dronsella, B., He, H., & Erb, T. J. (2024). Creating new-to-nature carbon fixation: A guide. *Metabolic Engineering*, *82*, 12–28. https://doi.org/10.1016/j.ymben.2023.12.012

Schwander, T., Schada von Borzyskowski, L., Burgener, S., Cortina, N. S., & Erb, T. J. (2016). A synthetic pathway for the fixation of carbon dioxide in vitro. *Science*, *354*(6314), 900–904. https://doi.org/10.1126/science.aah5237

Stettner, A. I., & Segrè, D. (2013). The cost of efficiency in energy metabolism. *Proceedings of the National Academy of Sciences*, *110*(24), 9629–9630. https://doi.org/10.1073/pnas.1307485110

Taylor-Kearney, L. J., Wang, R. Z., & Shih, P. M. (2024). Evolution and origins of rubisco. *Current Biology*, *34*(16), R764–R767. https://doi.org/10.1016/j.cub.2024.06.024

Thompson, M. G., Incha, M. R., Pearson, A. N., Schmidt, M., Sharpless, W. A., Eiben, C. B., Cruz-Morales, P., Blake-Hedges, J. M., Liu, Y., Adams, C. A., Haushalter, R. W., Krishna, R. N., Lichtner, P., Blank, L. M., Mukhopadhyay, A., Deutschbauer, A. M., Shih, P. M., & Keasling, J. D. (2020). Fatty Acid and Alcohol Metabolism in Pseudomonas putida: Functional Analysis Using Random Barcode Transposon Sequencing. *Applied and Environmental Microbiology*, *86*(21), e01665-20. https://doi.org/10.1128/AEM.01665-20

Volke, D. C., Friis, L., Wirth, N. T., Turlin, J., & Nikel, P. I. (2020). Synthetic control of plasmid replication enables target- and self-curing of vectors and expedites genome engineering of *Pseudomonas putida*. *Metabolic Engineering Communications*, *10*, e00126. https://doi.org/10.1016/j.mec.2020.e00126

Xin, C.-P., Tholen, D., Devloo, V., & Zhu, X.-G. (2015). The Benefits of Photorespiratory Bypasses: How Can They Work?1[OPEN]. *Plant Physiology*, *167*(2), 574–585. https://doi.org/10.1104/pp.114.248013

Zhang, W., Zhang, M., Gao, C., Zhang, Y., Ge, Y., Guo, S., Guo, X., Zhou, Z., Liu, Q., Zhang, Y., Ma, C., Tao, F., & Xu, P. (2017). Coupling between d-3-phosphoglycerate dehydrogenase and d-2-hydroxyglutarate dehydrogenase drives bacterial l-serine synthesis. *Proceedings of the National Academy of Sciences of the United States of America*, *114*(36), E7574–E7582. https://doi.org/10.1073/pnas.1619034114

6. Supplementary Material

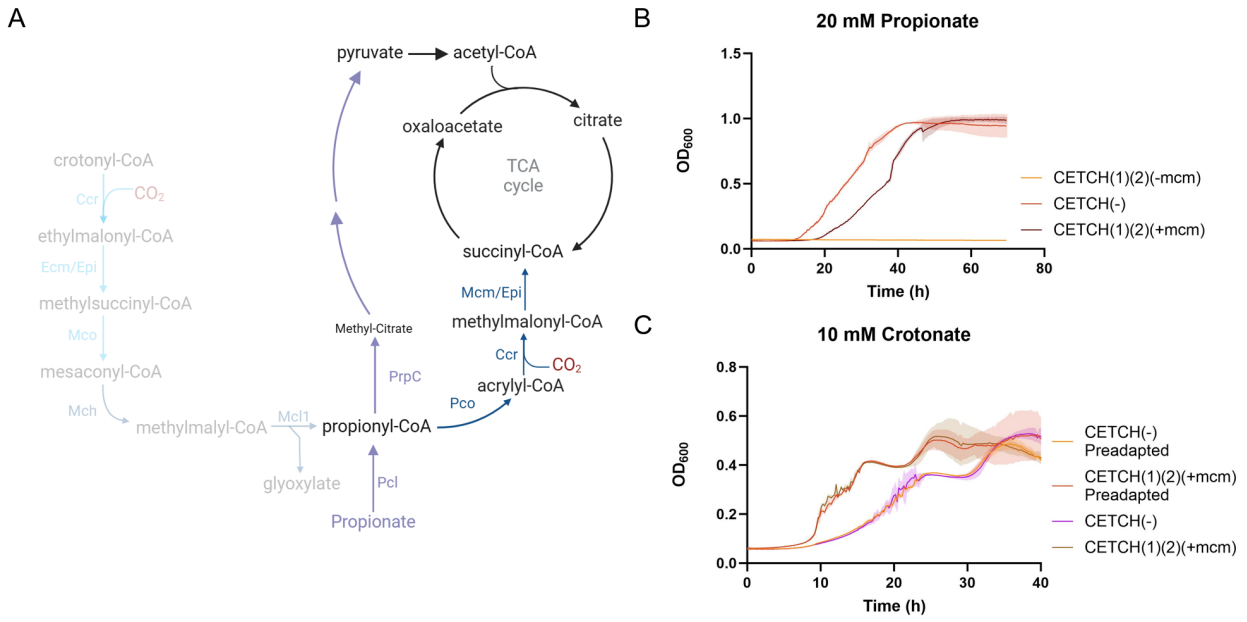

Figure S1 A) Schematic representation of propionate metabolism with the background of CETCH activities. Native activities in purple. PrpC: 2-methylcitrate synthase; Pcl: Propionyl-CoA ligase. B) Growth comparison of CETCH(-), CETCH(1)(2)(+mcm) and CETCH(1)(2)(-mcm) in 20 mM propionate. Shaded region represent the standard deviation of three technical replicates. C) Growth of crotonate-preadapted CETCH(-) and CETCH(1)(2)(+mcm) strains compared to their non-preadapted counterparts in 10 mM crotonate. Shaded region represent the standard deviation of three technical replicates.

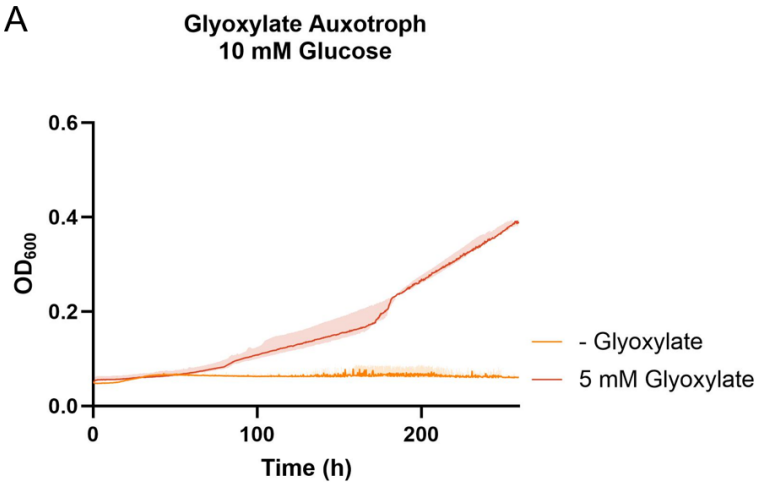

Figure S2 A Growth comparison of glyoxylate auxotroph in 10 mM Glucose with and without glyoxylate.